

A Non-iterative wavefront shaping method focusing light
through turbid media

Wang Siqi

June 2024

Contents

1	Introduction	3
2	Background	3
2.1	The historical background of the birth of wavefront shaping	3
2.2	The principle of wavefront shaping	4
2.3	Quantitative measures of enhancement	6
2.4	Types of modulations	7
2.5	Categorizations of spatial light modulators(SLMs)	9
2.6	Grouped iterations	9
2.6.1	Single-channel iteration	9
2.6.2	Grouped-channel iteration for higher SNR	10
2.6.3	Grouped-channel iteration for higher speed	13
3	The setup	15
4	Instant phase acquisition	17
4.1	Probing a channel	17
4.2	IQ demodulation	18
5	Position calibration	19
6	Phase calibration	24
7	Focusing light through turbid media	26
7.1	Result with (moving) glass diffuser	26
7.2	Result with a layer of milk	29
7.3	Result with a layer of corn starch	32
7.4	Result with multi-mode fibers	34

8	Conclusion and outlooks	38
8.1	The stability of the system	38
8.2	The observation of enhancement	38
8.3	The speed of optimization	39
8.4	Focus generation in turbid media	39

1 Introduction

In this thesis project, a non-iterative method of focusing light through (dynamic) turbid media is realized. The method is based on wavefront shaping, which is traditionally assisted by a time-consuming iterative process providing it with information necessary for optimization. In this project, instead of using an iterative process, a coherent probing arm and IQ demodulation are introduced in order to gather the information for optimization via an instant read-out manner. Thus, the time for optimization is in principle significantly reduced, allowing applications where dynamic turbid media are involved.

2 Background

Wavefront shaping has been indicated as a method for (partially) compensating for the effects of random scattering by modulating parameters such as phase, intensity, or polarization of the wavefront of the incoming light. A brief introduction concerning multiple aspects of this technique is given in the following subsections.

2.1 The historical background of the birth of wavefront shaping

To discuss the topic of wavefront shaping, it would be difficult to ignore an earlier-developed field called adaptive optics (AO). The story of AO started from the proposal by Horace W. Babcock, an American astronomer, in 1953 [3]. To correct the optical artifacts in astronomical data (e.g. atmospheric distortions, which are the most typical cause of the twinkle of stars), he suggested the use of a mirror covered by a thin film of oil with its shape controlled by local electron deposition in order to undo the blurring. Due to technical limitations, his idea did not become practical until the end of the 20th century when matured data processing methods and deformable mirrors allowing high-rate adjustments became available.

A typical AO imaging system works with the following scenario [2][4]: First, several luminous artificial guide stars are created in the visual field. For an astronomical telescope, the guide stars can be generated by having several points on the sodium layer of the atmosphere stimulated by orange laser beams. Known stars or other light emitting objects may also serve as guide stars. For AO assisted microscopy, a fluorescent bead embedded in the sample can be used. Then, light from the guide star is received by a wavefront sensor which measures the wavefront distortion (see figure 1 (a)). Based on the assumption that the optical distortion experienced by the light is weak, one can presume that the light from all points in a certain area of the visual field close to the guide star is similarly distorted as the light from the guide star. Therefore, at the third step, one can correct the whole area with a deformable mirror in accordance to the captured distortion (see figure 1 (b)).

The above correction can also be done purely by software [12]. Having a certain area of the visual field disturbed in the same way means the image in this area is convoluted by the same function. Since the shape of the artificial guide star is known, one can thus in principle find the convolution function in accordance to which a deconvolution can be performed via a division in Fourier space. Note that in case of low signal-to-noise ratio, the performance of the pure-software method is limited.

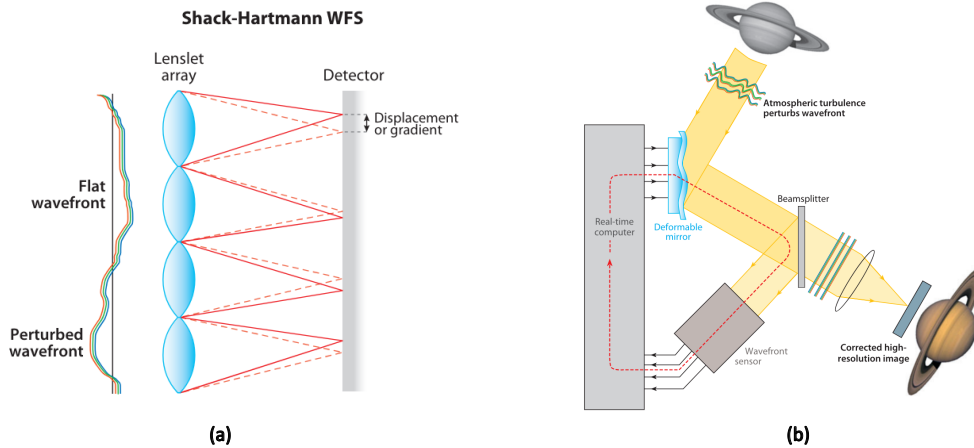


Figure 1: (a) A Shack-Hartmann wavefront sensor consisting of an array of lenses. For a tiny slice of the incoming wavefront, when it is parallel to the sensor surface, the corresponding focus will be on the axis of a lens. In case the tiny slice is tilted, the focus will be off axis [4]. (b) A typical layout of an AO telescope [4].

While both AO and wavefront shaping are about having the wavefront deformed in a certain way in order to compensate for unwanted effects, and the precise boundary between the two fields has not been clarified by far, it is still possible to conventionally divide them in accordance to their situations of application: AO is typically used to get rid of relatively weak optical distortions; wavefront shaping is usually applied for the cases where stronger and more complicated scatterings exist.

2.2 The principle of wavefront shaping

In 2007, Vellekoop et al. [13] proposed their new method of focusing coherent light through opaque media which is commonly seen as the first step of the wavefront shaping technique. The principle of their experiment is shown in Fig. 2.

Fig. 2 (a) describes the case where a spatial light modulator (SLM) acts as a simple mirror sending a coherent and monochromatic plane wave to a diffuser. When travelling through the diffuser, the light is randomly scattered multiple times, leaving a rather complicated configuration of paths. As a consequence, the outgoing wavefront is no longer in a “clean” plane-wave shape but rather strongly distorted.

When travelling through a diffusing material, the light in sufficiently adjacent paths will experience similar scattering effects. Therefore, it would make sense to spatially divide the incoming beam into multiple input channels. As shown in Fig. 2 (b), a certain input channel typically corresponds to multiple outputs.

It is possible to (at least partially) prevent the transmitted light from being scrambled by introducing

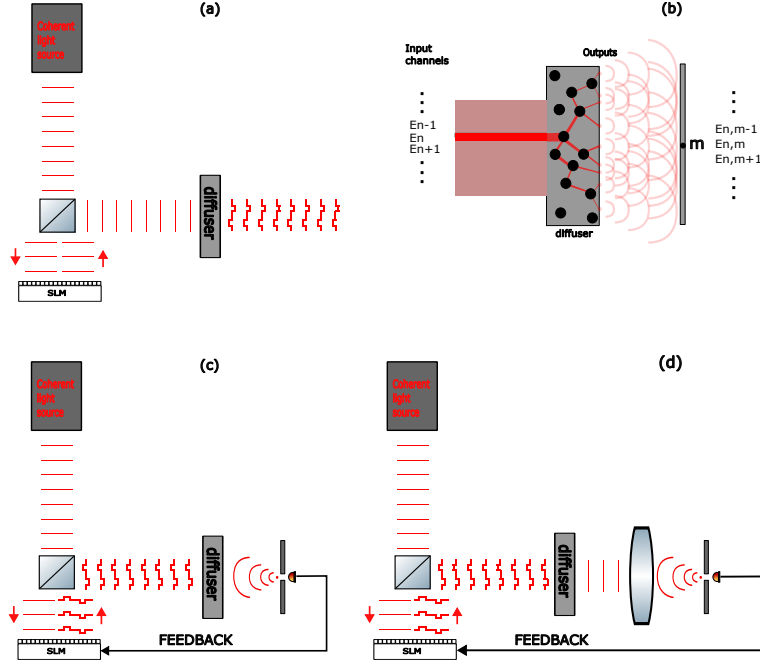


Figure 2: (a) Incident plane wave distorted by a diffuser; (b) The incident beam can be spatially divided into multiple channels where one channel corresponds to multiple outputs; (c) By modulating the incoming wavefront, one can have the light focused through turbid media; (d) Adding a lens and placing the sensor on its focal plane, one can in principle generate a plane outgoing wave by wavefront shaping;

a certain phase modulation at the SLM, as shown in Fig. 2 (c). By issuing a particular phase ϕ_n to the amplitude E_n of incoming channel n , one would be able to control the phase of $E_{n,m}$ which is the output amplitude of channel n at position m . In case this is done for all input channels, the interference at point m should be under a certain degree of control. With an appropriate set of ϕ_n , one can have the light from different channels constructively interfere at point m , thus a bright focus is generated. To emphasize “restoring” the incident plane wave, adding a lens behind the diffuser and placing the sensor on the focal plane of the lens shall work, as shown in Fig 2 (d).

However, it is normally not quite straightforward to find the correct phase configuration for such an optimization. In Vellekoop’s experiment, this was done via an iterative process: At each step of the iteration, the phases of part of the channels are modified, and the intensity at the site where a focus is supposed to arise is measured. The phase corresponding to the highest measured intensity is preserved. With this practice, the iteration will converge to the required phase configuration.

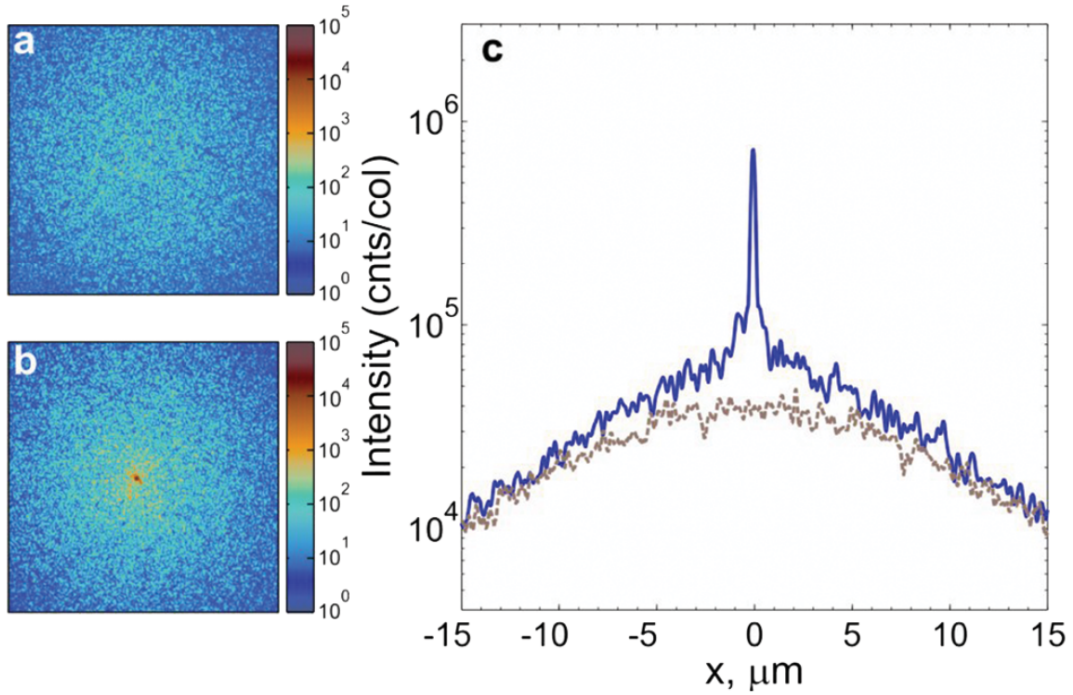


Figure 3: The work done by Vellekoop and A. P. Mosk in 2008 [14]. (a) An image of speckles before an optimization. (b) An image of speckles after an optimization. (c) Spatial distributions of intensities averaged along y direction. Dashed curve: intensity distribution for the image before the optimization. Solid curve: intensity distribution for the image after the optimization.

2.3 Quantitative measures of enhancement

To evaluate the performance of a focus generating method, a quantitative measure is required. The enhancement defined as follows is rather commonly used in the field of wavefront shaping [13]:

$$Enhancement = \frac{\text{Intensity of focus}}{\text{Averaged intensity before optimization}}$$

However, during the experiment of this project, the appearance of speckles surrounding the generated focus has been noticed. To take this into account, a slightly different definition of the enhancement is introduced:

$$Enhancement = \frac{\text{Intensity of focus}}{\text{Averaged background after optimization}}$$

The second definition above is supported by the work by I. M. Vellekoop and A. P. Mosk in 2008 [14], as shown in figure 3. One can see that the intensity after optimization is not only higher at the point where the focus is generated, but also higher in the proximity of the focus. This is due to the fact that optimization leads to a higher transmission by populating more transmissive channels in the medium.

2.4 Types of modulations

There exist multiple parameters of the incident light that one may manipulate while performing wavefront shaping. Correspondingly, different modulation methods are available [7].

It is possible to constructively enhance the interference at a certain field point by blocking part of the channels. A simplified situation is given in Fig. 4 (a). In this case, there are four channels contributing to the total amplitude E_m . While channel 1 to 3 are contributing positively to E_m (phasor angle difference less than $\frac{\pi}{2}$), channel 4 has a negative contribution to E_m (phasor angle difference more than $\frac{\pi}{2}$). Therefore, the absence of channel 4 would enhance the amplitude of E_m .

Instead of the removal of a channel with negative contribution, changing its phase by π would also enhance the total amplitude, as shown in Fig. 4 (b). Since no input channel is blocked in this case, one can expect the total enhancement to be typically higher than that of binary amplitude modulation.

The enhancement can be further increased by more delicately adjusting the phase of each channel, as described by Fig 4 (c). To increase the speed of an optimization, instead of having the phase of every channel continuously scanned, one can scan it with only several discrete phases. The enhancement achieved in this way shall be typically between that of binary phase modulation and continuously scanned full phase modulation. In practice, due to the existence of noise, the phase maximizing the amplitude might not be directly determined by the highest measured intensity. Otherwise, the intensity one records might be the sum of an overshoot of the noise and a non-maximized intensity. As an alternative, a phasor summation of intensities measured with different issued phases can be performed:

$$\tilde{I}_{\text{sum}} = \sum_i I(\phi_i)e^{i\phi_i}$$

As shown in figure 5, since the transversal components generally cancel, the direction of \tilde{I}_{sum} still approximately points in the direction of the maximum amplitude ($I(\phi_8e^{i\phi_8})$). Meanwhile, the noise (represented by green arrows) can be suppressed. The other way to deal with the noise is to extend the time of exposure. By doing this, the time integral of the signal will automatically have the noise suppressed. However, doing this will obviously lead to a decrease in optimization speed.

In 2015, Jongchan Park et al. proposed that the polarization of each input channel may also be regarded as a parameter to be modulated [10]. In this case, one input channel is splitted into two sub-channels, corresponding to the two orthogonal linear polarization components.

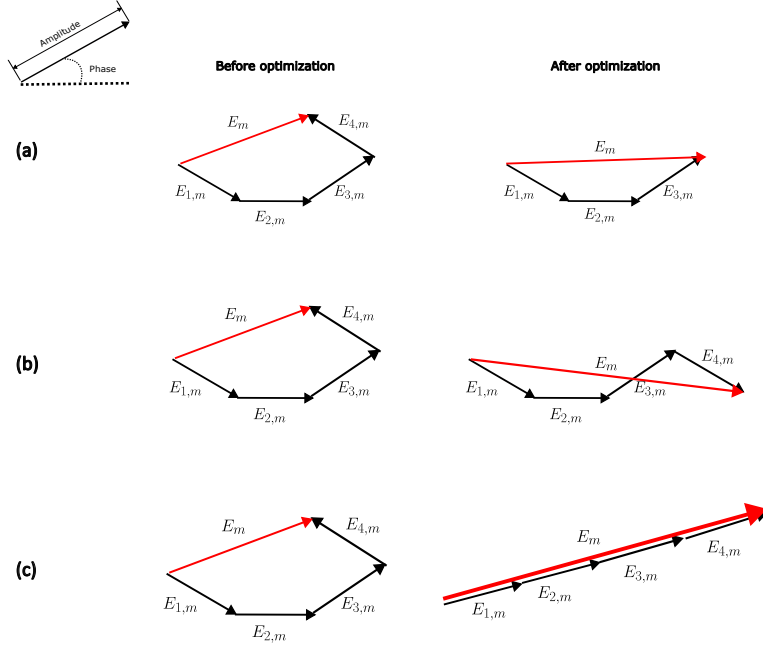


Figure 4: Types of modulations (a) Binary amplitude modulation. The enhancement can be increased by blocking channels contributing negatively; (b) Binary phase modulation. Instead of blocking negatively contributing channels, flipping their phasor directions may further increase the enhancement; (c) Full phase modulation. Delicate alignment of the phasor direction of all input channels in principle gives the highest enhancement;

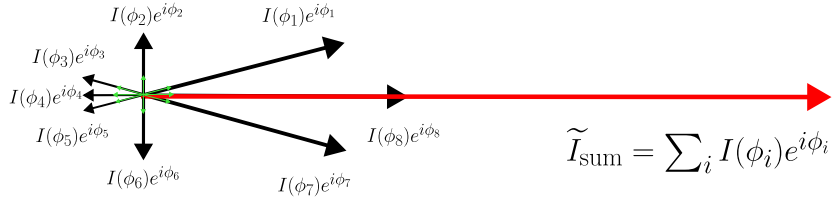


Figure 5: Compared to directly recording the phase corresponding to the highest observed intensity, taking the above phasor summation can better suppress the noise. The black phasors represent the intensities measured with different issued phases. The green phasors represent the noise involved in the above measurements. Due to the random nature of noise, the green phasors tend to cancel each other during the phasor summation. The red phasor stands for the phasor sum. The direction of the red phasor is supposed to be approximately the same as that of the phasor of the maximized amplitude. Note that this method works even if no sampled black phasor is pointing in the direction of the red phasor.

2.5 Categorizations of spatial light modulators(SLMs)

There exist multiple types of spatial light modulators with various features allowing different manners of modulation. Complying with one or another standard, one can put those SLMs under different categories[6].

In terms of the direction of outgoing light, SLMs can be sorted into two groups: reflective SLMs and transmissive SLMs. For the first type, the outgoing light and the incident light are on the same side of the SLM. For the second sort, the outgoing light and the incident light are different sides.

In terms of the principle of modulation, another categorization exists, including three most commonly used types listed as follows:

(1) The digital light processing (DLP) type. A typical DLP SLM is a rectangular array of millions of tiltable bistate micromirrors reflecting light in two directions one of which will be used for optimization while the other is directed to a beam dump. The most straightforward way of modulation for the DLP type is binary amplitude modulation. However, by using holographic techniques, it is also possible to perform phase modulation with a DLP SLM [9].

(2) The deformable mirror type. Instead of titling micromirrors, having the micromirrors composed of an array move upwards or downwards changes the length of the optical path of channels. Thus, a phase modulation can be performed. Deformable mirrors had been used for light modulation for decades before the birth of the wavefront shaping technique.

(3) The liquid crystal (LC) type. One can have more modulation modes by replacing the micromirror array by a controlled LC layer. Due to the anisotropic feature of LC molecules, the optical path length of the light traveling inside of the LC layer can change with the variation of the LC molecule orientation. This allows one to perform phase modulation. Besides, with the utilization of LC polarization rotation, a LC layer can also be used for intensity and polarization modulations.

While the DLP type and the deformable mirror type SLMs are generally known for their advantage of extremely high frame rates [9] [1] [15], ferroelectric liquid crystal SLMs are also capable to provide with a reasonably short response time.

2.6 Grouped iterations

Practically, it has turned out to be beneficial to have channels grouped in certain ways when optimizing iteratively in order to achieve higher signal-to-noise ratio (SNR) and higher speed.

2.6.1 Single-channel iteration

In principle, it is possible to scan only one channel per step. As an example, Fig. 6 demonstrates the iteration for six input channels with their phases iterated with this manner.

On each step, there is one and only one input channel having its phase scanned around 2π . The phase corresponding to the maximized total amplitude of the current step (i.e. when its phasor is in

the same direction as the sum of the other phasors) is preserved. After one round of such iteration, the total amplitude of the six channels has been significantly enhanced. From the figure, one can notice that the phasors of the channels iterated at the beginning are less perfectly aligned to the final result (compared to those optimized later). Therefore, it would make sense to iterate those channels once more after a whole round of optimization.

Practically, the noise can be a rather significant problem for single-channel iterations. Since there is only one channel scanned per step, the measured intensity change would typically not be high. Therefore, the signal to noise ratio (SNR) may suffer.

2.6.2 Grouped-channel iteration for higher SNR

One way to increase the SNR is to have multiple channels grouped and scanned with fixed relative phases. Since the phasor summation of multiple channels would have a nontrivial chance to generate an amplitude significantly higher than that of a single channel, the intensity change measured in this case will typically have a stronger contrast.

One can use an Hadamard transform to perform the above grouping [8][1]. A simplified example of grouping 4 input channels with an order 4 Hadamard matrix is given as follows:

Without loss of generality, the phase of the reference can be defined to be 0. Based on this, the field of the four modulated channels is written as:

$$\begin{aligned}\tilde{E}_1 &= E_1 e^{i\Phi_1} \\ \tilde{E}_2 &= E_2 e^{i\Phi_2} \\ \tilde{E}_3 &= E_3 e^{i\Phi_3} \\ \tilde{E}_4 &= E_4 e^{i\Phi_4}\end{aligned}$$

With the above basis one can perform the following Hadamard transform:

$$\begin{bmatrix} \tilde{E}_{H1} \\ \tilde{E}_{H2} \\ \tilde{E}_{H3} \\ \tilde{E}_{H4} \end{bmatrix} = \begin{bmatrix} 1 & 1 & 1 & 1 \\ 1 & -1 & 1 & -1 \\ 1 & 1 & -1 & -1 \\ 1 & -1 & -1 & 1 \end{bmatrix} \cdot \begin{bmatrix} \tilde{E}_1 \\ \tilde{E}_2 \\ \tilde{E}_3 \\ \tilde{E}_4 \end{bmatrix}$$

or

$$\begin{bmatrix} E_{H1} e^{i\Phi_{H1}} \\ E_{H2} e^{i\Phi_{H2}} \\ E_{H3} e^{i\Phi_{H3}} \\ E_{H4} e^{i\Phi_{H4}} \end{bmatrix} = \begin{bmatrix} 1 & 1 & 1 & 1 \\ 1 & -1 & 1 & -1 \\ 1 & 1 & -1 & -1 \\ 1 & -1 & -1 & 1 \end{bmatrix} \cdot \begin{bmatrix} E_1 e^{i\Phi_1} \\ E_2 e^{i\Phi_2} \\ E_3 e^{i\Phi_3} \\ E_4 e^{i\Phi_4} \end{bmatrix}$$

where index j indicates the j th channel involved in the transform, and index H_j indicates the j th Hadamard basis. As shown in figure 7, the amplitude of the transformed basis is typically higher than that of the original basis. When a higher amplitude is modulated, one can expect to see a larger SNR.

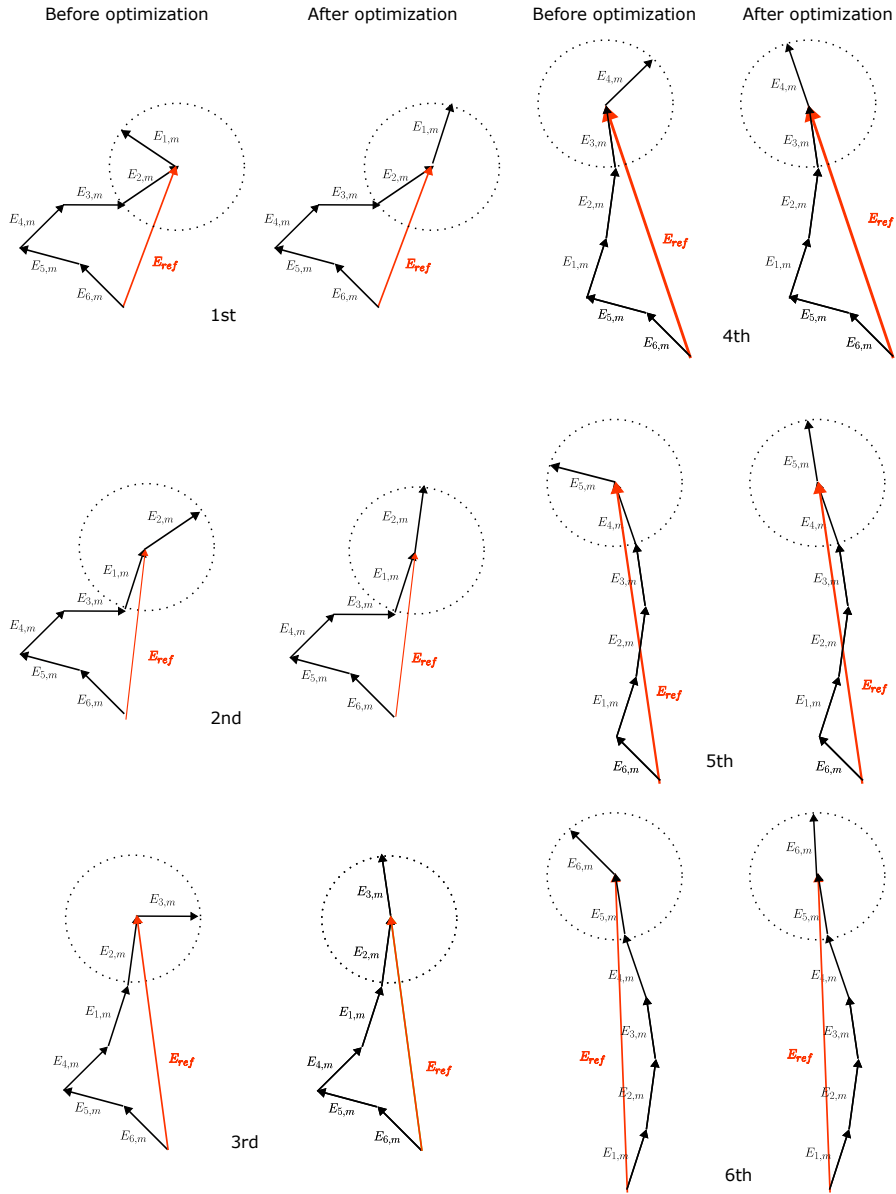


Figure 6: Here the optimization is done channel by channel. Compared to that of grouped iterations, the signal acquired here is relatively low. This will lead to a typically low SNR.

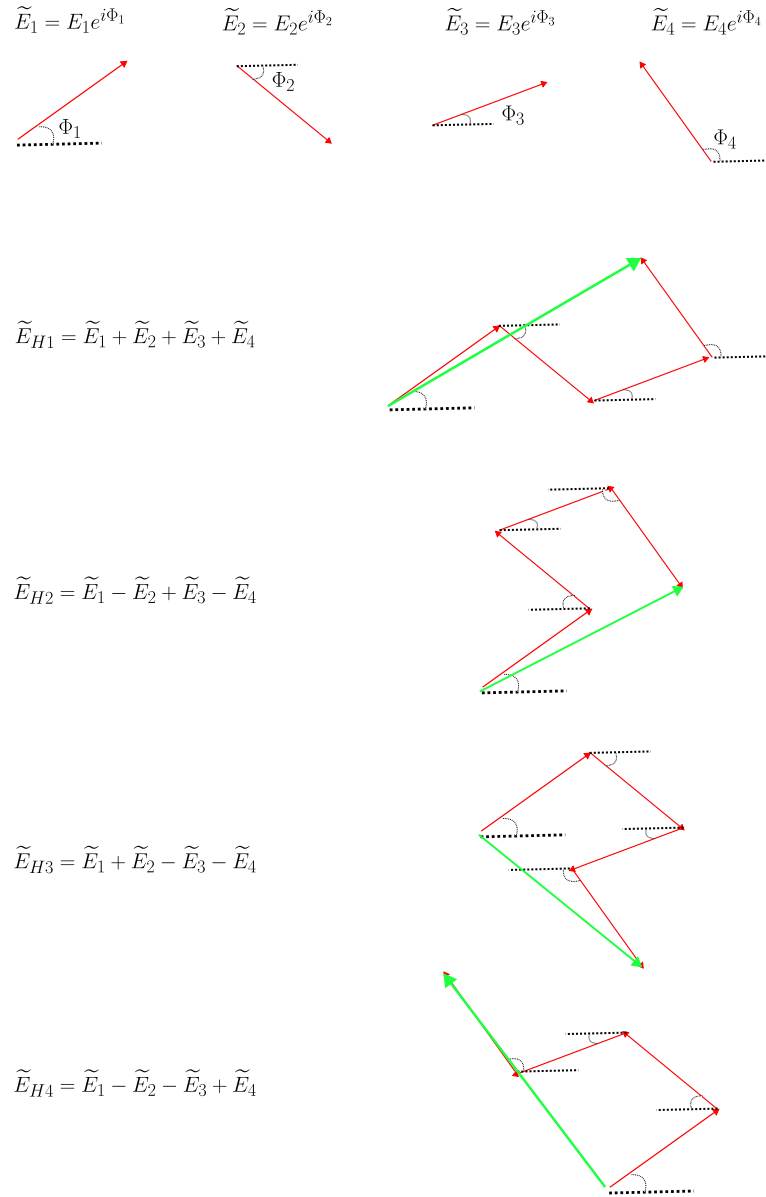


Figure 7: Here is an example of Hadamard transform. 4 original bases are transformed into 4 Hadamard bases. The amplitude of a transformed basis is rather likely to be higher than that of an original basis. Therefore, the signal acquired during modulations after Hadamard transforms is typically higher, and such a modulation typically gives better SNR. One can notice that the number of modulations cannot be reduced by an Hadamard transform.

By performing iterative optimization upon the Hadamard basis, one is able to obtain $[E_{Hj}e^{\Phi_{Hj}}]$, with which it one can get $[E_j e^{\Phi_{hj}}]$ through an inverse Hadamard transform. Thanks to the "involutory" nature of Hadamard matrices, this can be done in a rather straightforward way:

$$\begin{bmatrix} E_1 e^{i\Phi_1} \\ E_2 e^{i\Phi_2} \\ E_3 e^{i\Phi_3} \\ E_4 e^{i\Phi_4} \end{bmatrix} = \frac{1}{4} \begin{bmatrix} 1 & 1 & 1 & 1 \\ 1 & -1 & 1 & -1 \\ 1 & 1 & -1 & -1 \\ 1 & -1 & -1 & 1 \end{bmatrix} \cdot \begin{bmatrix} \tilde{E}_{H1} \\ \tilde{E}_{H2} \\ \tilde{E}_{H3} \\ \tilde{E}_{H4} \end{bmatrix}$$

Thus, Φ_1 , Φ_2 , Φ_3 and Φ_4 are known. According to this, one can have the phasors of channels 1 to 4 aligned to the direction of the reference.

Note that a Hadamard transform would not be able to speed up the iterative process. Since the number of transformed vectors is equal to the number of channels involved, the number of steps in this manner is not going to be less than that of a single-channel iteration. However, because of the high SNR, one might be able reduce the time of exposure. This can indirectly reduce the time for a focus generation.

2.6.3 Grouped-channel iteration for higher speed

Beyond the enhancement of SNR, having channels grouped may also achieve a higher speed. For this purpose, instead of performing transforms (i.e. an Hadamard transform), one can simply have several pixels on the SLM combined into a coarser segment. While having less fine segments for modulation will in principle reduce the enhancement, in a certain region of coarseness such reduction can be trivial. Figure 8 shows the enhancement results with varying coarseness recorded by Vellekoop et al. [13].

The solid straight line stands for a preliminary estimation that the enhancement obtained with N segments is supposed to be linearly dependent to N: Supposing the intensity of all channels are identical ($= E$), taking the sum of N randomly oriented phasors resembles finding the final result of a N-step random walk which gives an expected value of $\sqrt{N}E$. For N fully optimized phasors, the total amplitude is NE . Therefore, the estimated enhancement is

$$\frac{E_{\text{Optimized}}^2}{E_{\text{Non-optimized}}^2} = \frac{(NE)^2}{(\sqrt{N}E)^2} = N$$

Notice that the enhancement here is defined in the first way introduced in section 2.3. The dashed curve stands for a correction including a finite speckle persistence time:

$$\text{Effective enhancement} = \frac{\text{Ideal enhancement}}{1 + \frac{NT}{T_p}}$$

where T is the time required for updating a segment, and T_p is the persistence time of the speckle pattern. In Vellekoop's experiment, T is around 1.2s, and T_p is found to be around 5400s for their TiO_2 pigment sample. The persistence time for a dynamic diffusing sample can be significantly shorter. The recorded enhancements are indicated by squares and triangles. The squares stand for the situation where the sample is placed in focus; the triangles are used for the case where the sample is 100 micrometers behind the focus. One can notice that at high number of N, the recorded data

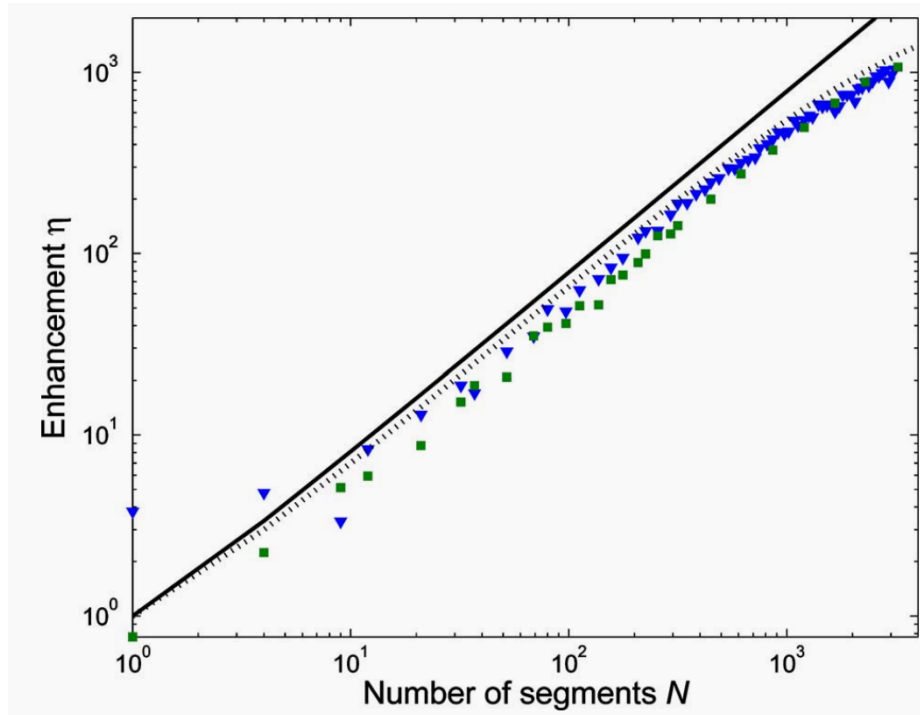


Figure 8: A saturation is found by Vellekoop et al. [13] when segments become sufficiently fine.

complies with the dashed curve rather well. This implies that, due to the limited rate of segment update and the instability of the sample, having a too high number of segments will increase the difficulty for the system to follow the changes of the sample.

Even if the rate of segment update was sufficiently high, one might still foresee another cause of saturation at a high number of segments. When the transmitting light is divided into extremely fine channels, a phase correlation among neighbouring channels will appear. In this case, optimizations of a bunch of neighbouring channels will give almost the same phase, which can be obtained with a larger segment size.

3 The setup

In the experiment of this project, a 589nm laser serves as the coherent light source. Light leaving from the source travels through an acousto-optic tunable filter (AOTF) where an additional beam with a 103.086 MHz frequency deviation is created. A 512*512 liquid crystal spatial light modulator (SLM) provided by Meadowlark Optics enables phase modulations with a particularly high rate.

The layout of the setup is given in Figure 9. One can divide the optical part of the setup into two arms: the modulated arm (in orange) and the probing arm (in yellow). The lengths of the two arms are designed to be similar in order to have the spatial coherence preserved.

The modulated arm comes from the 0th order output of the AOTF (i.e. no change of frequency). It is first re-shaped by a spatial filter L1-P1-L2 into a plane wave, and then imaged on the SLM by another typical 4f system L3-L4. Thus a certain area of the SLM surface is illuminated, and the pixels (or segments) included in this area can participate in the optimization. The surface of the SLM is imaged to the surface of the diffuser by lens L9, so that every pixel (or segment) of the SLM is corresponded to one of input channels.

The probing arm comes from the 1st order output of the AOTF, and its frequency is 103.086 MHz higher than that of the modulated arm. Similarly, the beam is first shaped by L5-P2-L6, and then sent to M1-L7-M2, which generates a focus on the lateral plane LP1 where lens L8 is placed. The position of the focus is solely determined by the angular position of tiltable mirrors M1 and M2, and vice versa. The focus on LP1 is imaged virtually at a certain point on the SLM surface by a beam splitter (BS), thus the probing light coming out of BS should geometrically coincide with the light coming from the point on the SLM.

One may notice that with the above layout, it is inevitable to have a nonzero angle between the virtual image of LP1 and the surface of the SLM. This can be overcome by a phase calibration of the probing arm (see the section on calibration). The same calibration can also correct the phase deviation contributed by the rotation of the mirrors (mainly including two effects: (1) The rotation axis of mirrors do not go through the surface; (2) The path length of beam changes with scanning angle;).

A pinhole (or an iris) is placed in the space behind the diffuser, determining the position of the generated focus. The size of the pinhole is chosen to be comparable to that of the random speckles. Light entering the pinhole is the compound of light for the modulations and probing light with its frequency shifted by 103.086MHz. Thus, a beat with the frequency 103.086 MHz is formed. One can show that the phase of the beat is the same as the phase of the probed channel (or the probing light). A J-Series type 30035 silicon photomultiplier (SiPM) provided by SensL (Osemi) serves as the sensor. 5676 microcells are integrated in the SiPM, and the time for a single cell recovery is around 45 ns. With a relatively fast speed of recovery and a sufficiently high number of cells, the SiPM is capable of monitoring the beat. The signal of the beat is passed to an analogue IQ demodulator, where the phase is extracted in a manner similar to a lock-in amplifier.

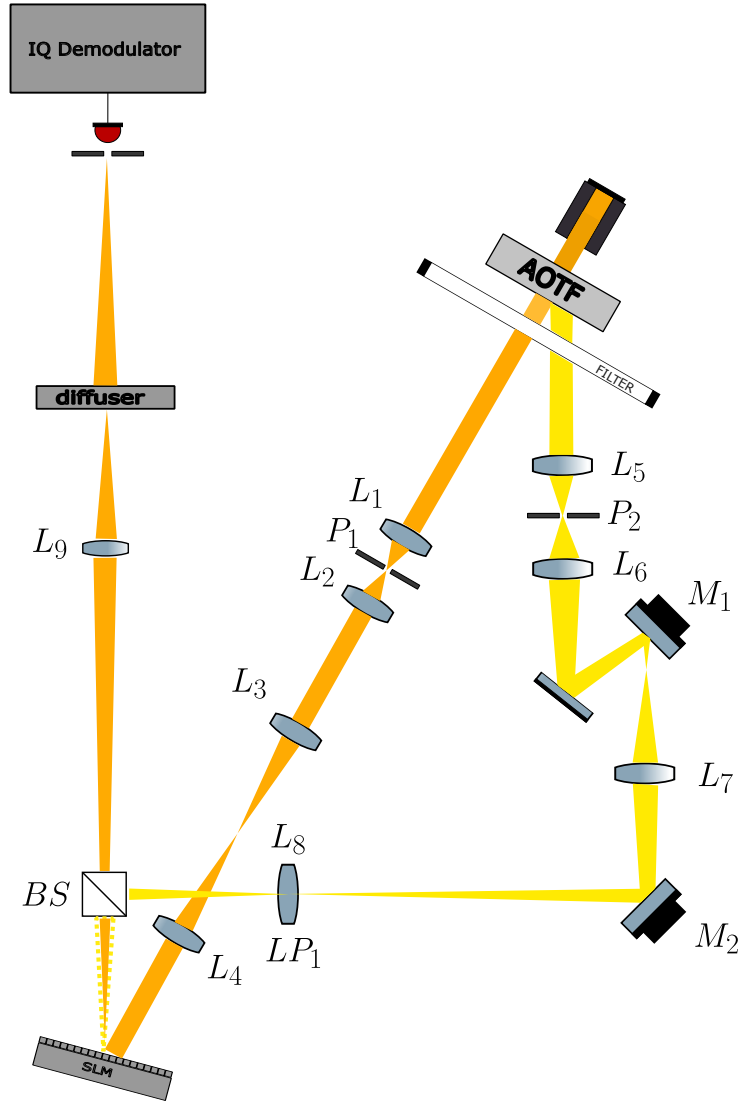


Figure 9: The figure above gives the general layout of the setup. The setup can be roughly divided into two branches: the modulated arm (in orange color) and the probing arm (in yellow color). The difference in color implies a 103.086MHz frequency shift introduced by the AOTF. For the modulated arm, between the light source and the SLM, the whole bunch of light is included in the figure. To better illustrate the fact that the illuminated area of the SLM is imaged on the surface of the diffuser, between the above two components, a point-to-point convention of sketching is used.

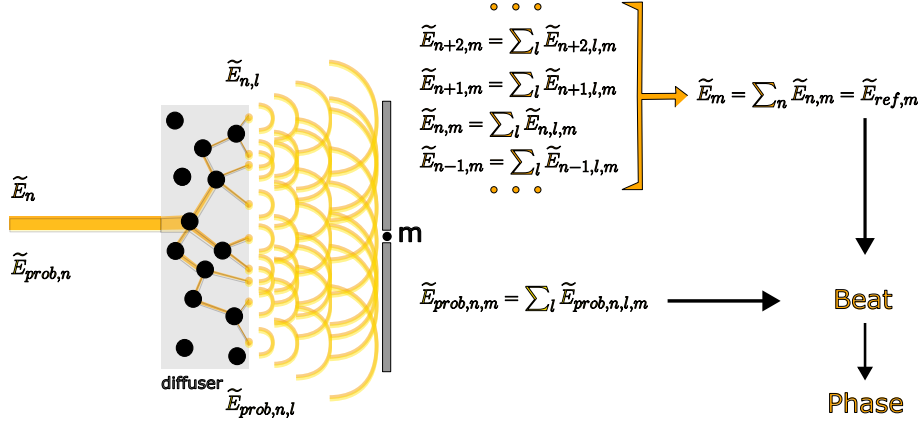


Figure 10: Sufficiently adjacent input beam lines can be included in the same input channel. One channel is typically corresponded to multiple outputs which interfere in the space behind the diffuser. Supposing at a specific point of interest behind the diffuser, the interference of the outputs corresponding to a certain input channel is destructive, then this specific input channel cannot be involved in the optimization for generating a focus at the specific point.

4 Instant phase acquisition

In this project, the phase information for optimizations is acquired via instant measurements instead of iterations. The principle of the phase acquisition is given in this section.

4.1 Probing a channel

As shown in figure 10, the incident light (in orange) can be divided into multiple input channels, and each channel is related to multiple outputs. The waves from the outputs shall interfere in the space behind the diffuser. At point m , the amplitude contributed by input channel n ($E_{n,m}$) is supposed to be the phasor sum contributed by all outputs:

$$\tilde{E}_{n,m} = \sum_l \tilde{E}_{n,l,m}$$

where the label l is used to indicate different outputs of channel n .

While $\tilde{E}_{n,l,m}$ with different l normally have different phases, their relative phases are supposed to be invariant. Therefore, changing the phase of the input channel n is not about to modify the relative phases of its outputs. In case the amplitude $\tilde{E}_{n,m}$ is too low due to destructive interference, channel n would not be available for the optimization. This can be considered as one of the performance limits of phase-only modulations. Practically, it would be typically beneficial to reduce the size of the image of the SLM on the surface of the diffusing sample.

When the probing arm (in yellow) coincides with the input channel n , the probing light experiences the same scattering as that of the light of channel n . Therefore, knowing the phase of the probing light ($\tilde{E}_{\text{prob } n,m}$) is equivalent to knowing the phase of $\tilde{E}_{n,m}$. The phasor sum of the amplitudes contributed by all input channels serves as the reference ($\tilde{E}_{\text{ref } m}$) for phase measurements. Due to the 103.086 MHz frequency deviation between the probing arm and the modulated arm, a beat of that frequency is formed. The phase of the beat relative to $\tilde{E}_{\text{ref } m}$ is supposed to be the same to the phase of $\tilde{E}_{\text{prob } n,m}$. A proof is given as follows.

Supposing the phase of $\tilde{E}_{\text{prob},n,m}$ is $\phi_{n,m}$ with respect to $\tilde{E}_{\text{ref},m}$, one can choose:

$$\begin{aligned}\tilde{E}_{\text{prob},n,m} &= E_{\text{prob},n,m} e^{i\phi_{n,m}} e^{i\omega_{\text{prob}}t} \\ \tilde{E}_{\text{ref},m} &= E_{\text{ref},m} e^{i\omega t}\end{aligned}$$

where ω_{prob} is the frequency of the probing arm and ω is the frequency of the modulated arm. The interference of the above two vectors gives:

$$\begin{aligned}I_{\text{interference}} &= (\tilde{E}_{\text{prob},n,m} + \tilde{E}_{\text{ref},m})^2 \\ &= E_{\text{prob},n,m}^2 + E_{\text{ref},m}^2 + E_{\text{prob},n,m} E_{\text{ref},m} [e^{i(\omega_{\text{prob}} - \omega)t + i\phi_n} + e^{i(\omega - \omega_{\text{prob}})t - i\phi_n}] \\ &= E_{\text{prob},n,m}^2 + E_{\text{ref},m}^2 + 2 \cos[(\omega_{\text{prob}} - \omega)t + \phi_n]\end{aligned}$$

One can filter out the above DC terms ($E_{\text{prob},n,m}^2 + E_{\text{ref},m}^2$), and the remaining term $2 \cos[(\omega_{\text{prob}} - \omega)t + \phi_n]$ stands for a beat with a frequency ($\omega_{\text{prob}} - \omega$) and a phase ϕ_n . Notice that the phase of the beat is exactly the same as the phase of the probing light.

4.2 IQ demodulation

To read out the phase of the beat (i.e. the phase of the measured channel), IQ demodulation is introduced, which measures the amplitude projections of the signal on both sinusoidal and cosinusoidal bases in a lock-in manner. This is equivalent to the acquisition of the phase of the signal. A proof of the equivalence is given as follows.

Given $\tilde{y} = y \cos(\omega x + \phi)$ as the signal, one has:

$$\tilde{y} = y[\sin(\phi) \cos(\omega x) + \cos(\phi) \sin(\omega x)]$$

Supposing the value acquired from the lock-in measurements on sinusoidal and cosinusoidal bases are respectively:

$$A = Cy \cos(\phi)$$

and

$$B = Cy \sin(\phi)$$

where C is the gain of the lock-in amplification. Than one should have:

$$\phi = \arctan\left(\frac{B}{A}\right)$$

In this way, the phase of a certain channel can be acquired. By having all channels scanned in the same manner, one can instantly gather the phase information required for an optimization and have them compensated by the SLM.

Practically, the signal sent to the AOTF is used as the demodulation signal. Thus, an additional phase between the probing arm and the demodulation signal can be introduced. However, since such a phase change is uniform for all input channels, in principle, no correction is required.

5 Position calibration

To have all channels scanned for an optimization, the probing arm is guided by a pair of oscillating mirrors (one fast and one slow, $f_{\text{fast}}=4\text{kHz}$, $f_{\text{slow}}=1/64 f_{\text{fast}}$), which have the probing light enter all scanned channels for once during a scanning period, as shown in figure 11 (a). While as discussed in section 3, the spatial positions of the probed channel and the angular positions of the mirrors have a one-to-one correspondence, the dependence does not seem to be linear. Therefore, to find out which channel is currently scanned, and correspondingly, to determine which pixel (or segment) of the SLM needs to be adjusted, one would need a position calibration. The setup layout used for position calibration is given in figure 11

The main point of a position calibration is to have the signal from a selected part of the channels more conspicuous, so that when this area is scanned, a change in the signal can be noticed. With this, one can figure out which angular position of the mirrors is related to which specific position on the SLM. This can be achieved by spatial low-pass filtering [5], and its principle is given below:

Having the pattern on the SLM illuminated by a coherent plane wave, and having the outgoing light transformed by lens L9 (i.e. the condition for Fraunhofer diffraction is met), one can expect to see the Fourier transform of this pattern on the lateral plane where iris P3 is placed.

Supposing a checkerboard pattern is written on the SLM where neighboring squares differ by a phase of π (Fig. 12 (a)), the transformed pattern shown in figure 12 (d) should be found at P3. Due to the high spatial frequency of the checkerboard pattern, the low frequency component (i.e. the central part of the transform pattern) is relatively weak.

In case a stripe (with a constant phase, i.e. with a relatively low spatial frequency) is written over the checkerboard pattern, as shown in figure 12 (b), the center of the transformed pattern would be enhanced. By optically filtering out the high-frequency components (Fig. 12 (f)), one can strongly emphasize the signal from the stripe (Fig 12 (c)).

In the experiment, moving stripes perpendicular to the slow and fast axes respectively are used to calibrate the slow and fast mirrors, as shown in figure 13. Note that while the fast mirror is oscillating almost freely with its 4kHz frequency, the slow mirror is controlled and synchronized to the motion of the fast mirror. Therefore, knowing the time of an event is equivalent to knowing the corresponding angular position of the mirrors.

Figure 13 (a) describes the calibration for the slow mirror. The surface of the SLM is scanned by a stripe moving along the slow axis, and the scanning is sufficiently slow to have the mirrors probe the whole surface for each step of the stripe. When the probing light touches the stripe, a high signal of

the 103.086 MHz beat can be detected, which is indicated by the solid bar in the right-hand -side chart. With the scan going, all dashed bars are gradually filled. Thus, one can perform a linear fit, which matches up the time and the position along the slow axis. Further, one can find the correspondence of the slow axis position to the angular position of the slow mirror.

Figure 13 (b) shows the calibration for the fast mirror, with the stripe moving along the fast axis. In this case, high-signal-points are filled into a sinusoidal-like curve. After the scan, the completed curve is fit with a sinusoidal function. An extra linear term may be added to the function for fitting in order to correct the imperfect alignment of the mirrors.

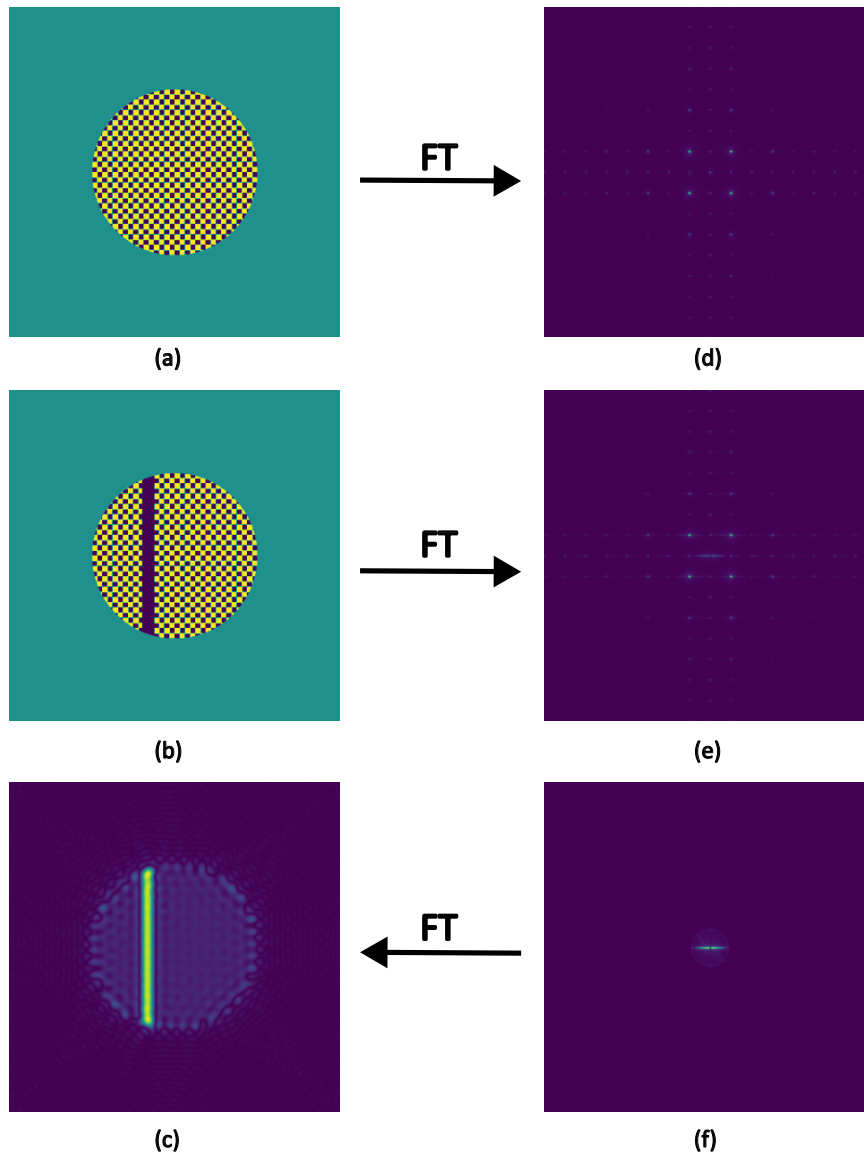


Figure 12: Here is a simulation of the spatial filtering. (a): A checkerboard pattern partially illuminated by the incoming light; (d): The Fourier transform of the checkerboard pattern; (b): Overwriting a stripe with uniform phase on the checkerboard pattern; (e): The Fourier transform of the pattern in (b). One shall notice its low frequency component (i.e. the central part of the figure) is brighter than that of (d); (f): Having the high frequency component of (e) filtered out; (c): The (inverse) Fourier transform of the pattern in (e). In the restored pattern, the stripe is emphasized in terms of intensity; Note that (a) and (b) are plots of amplitude (yellow = 1, dark blue = -1 and aqua green = 0), and (c), (d), (e) and (f) are plotted in accordance to absolute values.

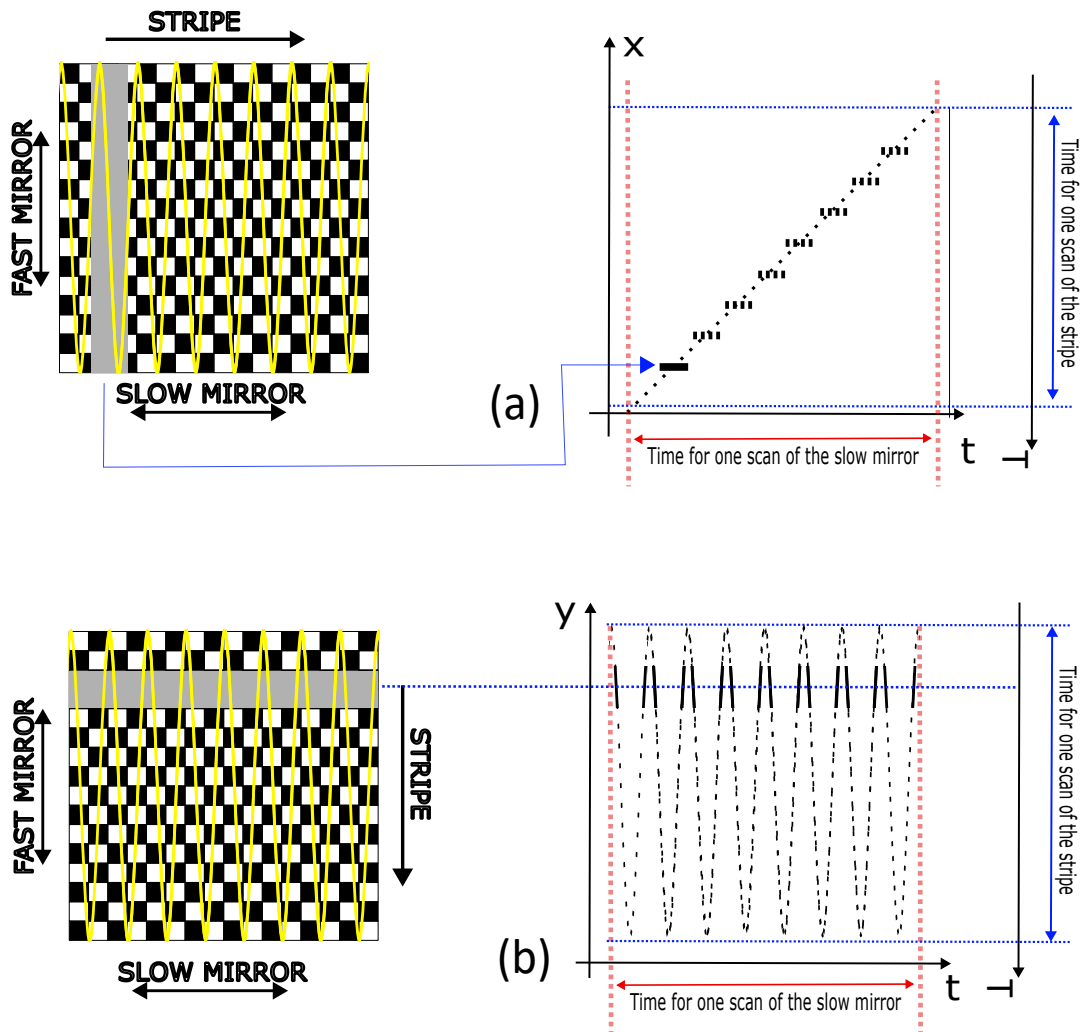


Figure 13: (a): The calibration scan for the slow mirror; (b) The calibration scan for the fast mirror; Again, the checkerboard in the figure is not to scale.

6 Phase calibration

Beyond the calibration of mirror position, another calibration is introduced for the correction of multiple problems:

- (1) Flatness issue of the SLM. While in principle the surface of a non-modulating SLM is supposed to be flat, practically, it is possible to have tiny imperfectness when a real piece is fabricated.
- (2) Phase deviation introduced by the probing arm. When a mirror is tilted to the side, the light would travel a little bit longer to reach the next component than that of the case where the mirror is at the central angular position. While this is partially mitigated by the lens right before the beam splitter, a finer compensation is still necessary.
- (3) Imperfect flatness of the incident plane wave. During the construction of the setup, the wavefront flatness is qualitatively checked and handled by using a shearing interferometer. However, the light illuminating the SLM can still be slightly diverging or converging.

The above listed problems can be fixed by forming a lookup table issuing each specific channel a specific offset compensating for the phase deviations regardless their sources of origin. One can obtain the lookup table via the following steps:

First, write a reference phase pattern on the SLM;

Second, measure the phase of the channels with the uncalibrated setup;

Third, subtract the measured phase pattern by the known phase pattern, and the result will be the lookup table;

In this project, the reference phase pattern is chosen to be one generating a focus in free space. The setup layout for its acquisition is given in figure 14.

The reference phase pattern is acquired via an traditional iterative process. As discussed in section 2.4, for better convergence, the iteration is executed twice. While the probing arm is not used during the iteration, to avoid additional deviations in phase, the AOTF remains on, and the probing beam is blocked to avoid it affecting the iteration.

The distance between the beam splitter and pinhole P3 should be as long as possible, that the spatial frequency of the phase pattern acquired via the iteration can be reduced. Thus, the reference can be more robust against noise. As shown in figure 15 (a), the original reference phase pattern normally comes with high frequency noise. To remove the noise, one can blur the whole array using a Gaussian. The result is given in figure 15 (b). While one may argue that the Gaussian blurring can affect the compensation of the flatness issue of the SLM, for the specific device used in this project, flatness problems are only expected to happen on a larger spatial scale.

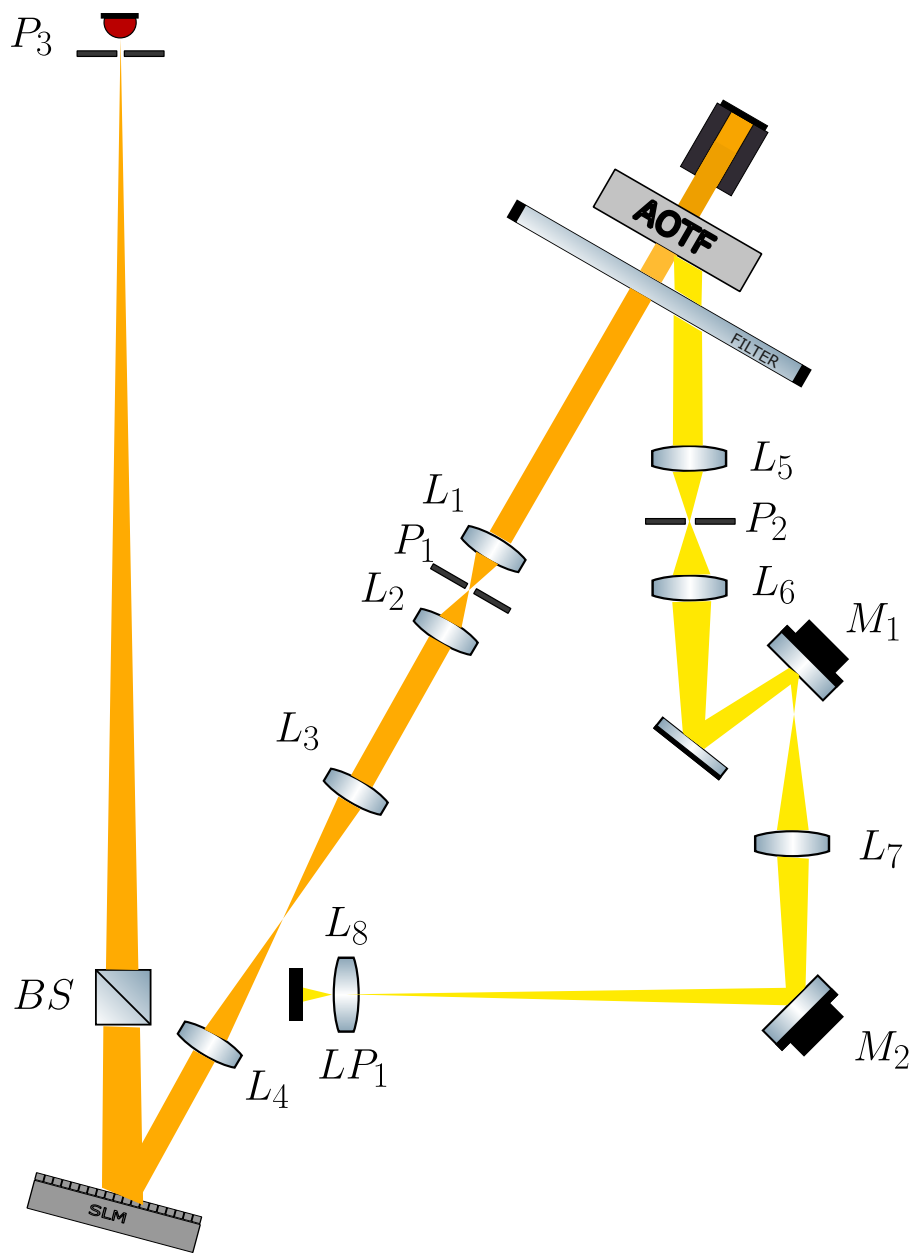


Figure 14: The set up for the acquisition of the phase reference. While the probing arm (in yellow color) is blocked, the AOTF remains to be on in order to avoid additional phase deviations.

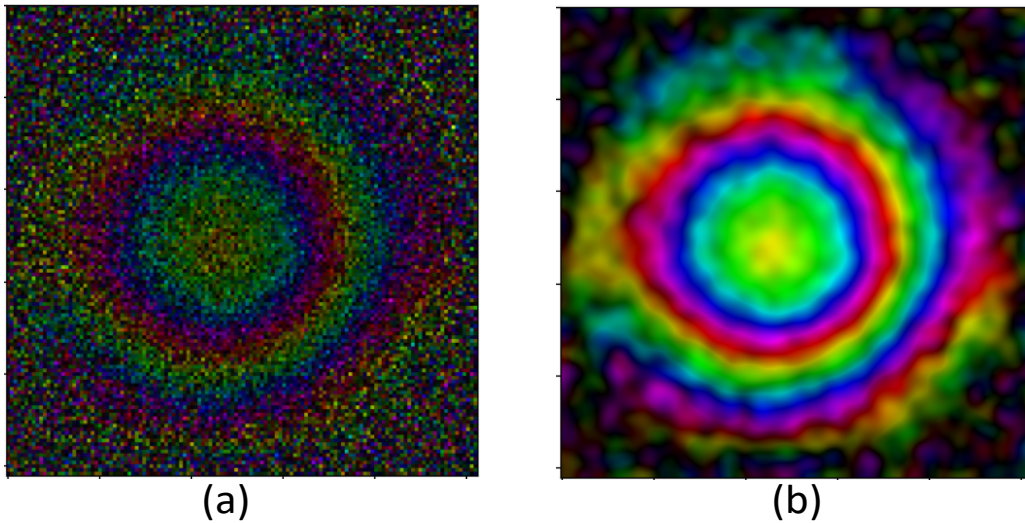


Figure 15: The phase reference. (a): The original phase pattern obtained from an iteration; (b): Having the phase pattern in (a) blurred by a Gaussian function in order to suppress the noise;

7 Focusing light through turbid media

With the setup built and calibrated as described in the above sections, focus generations through multiple sorts of turbid media are now attempted. The results are given in the following subsections.

7.1 Result with (moving) glass diffuser

The sample for the first attempt is a piece of glass diffuser mounted on a movable stage. An additional beam splitter and a CCD camera are added to monitor the enhancement, as shown in figure 16. The distances l_1 and l_2 are kept the same in order to have the speckle pattern (including the case of having a focus) at P3 properly imaged on the CCD. The optimizations are performed with different speeds of the glass diffuser, varying from 0 micrometers per second to 100 micrometers per second. The histograms of the enhancements acquired with different speeds are given in figure 17. Each histogram contains 2000 samples distributed into 100 bins.

The six histograms given on the top (labeled as “Fixed position 0 to 5”) demonstrate the enhancement distributions acquired at six arbitrary positions behind a fixed glass diffuser. One can notice that the enhancement distributions vary in response to the change of position. This indicates a sample-dependence of the setup performance.

The enhancement distributions acquired with speed between 10 and 100 micrometers per second are given in the lower ten histograms (labeled as “Speed 10 to 100” respectively). A clear trend of

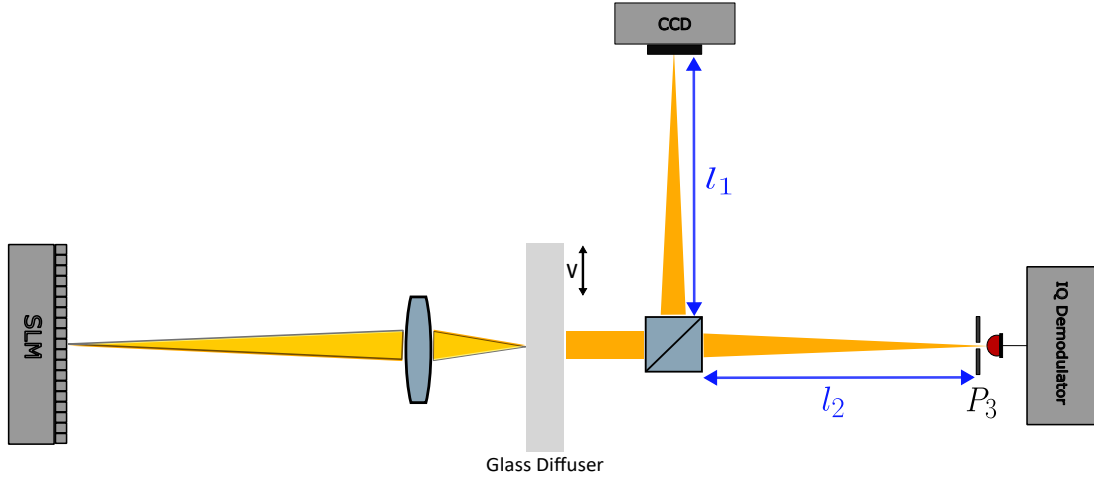


Figure 16: Focusing through glass diffuser

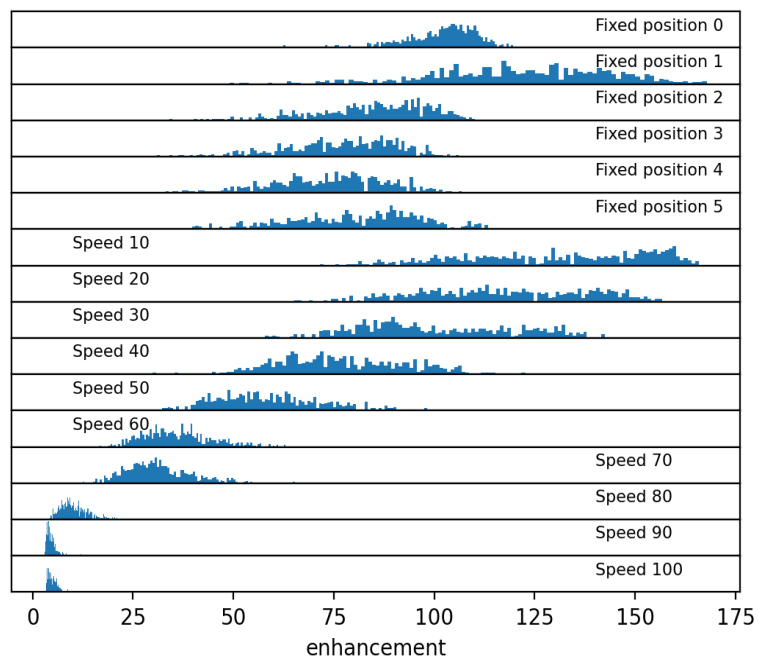
negative correlation between the speed and the enhancement exists.

One can see from figure 17 (b) that up to the sample speed of $60\mu m \cdot s^{-1}$, a decent focus can be generated. The length scale on which correlation exists is estimated to be around $10\mu m$. So the approximate upper limit of the speed this setup can handle is around:

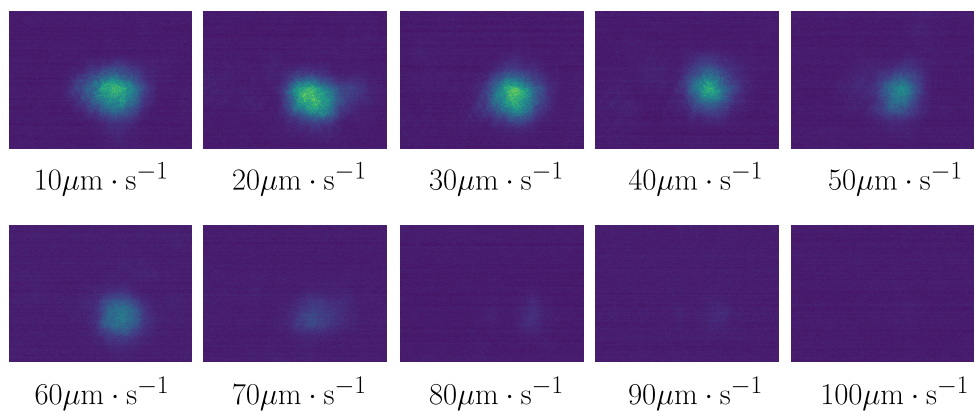
$$\frac{v_{max}}{l_{correlation}} = \frac{60\mu m \cdot s^{-1}}{10\mu m} = 6s^{-1}$$

and correspondingly, the shortest time scale it can react to is:

$$\frac{1}{6s^{-1}} \approx 0.17s$$



(a)



(b)

Figure 17: Results with glass diffuser

7.2 Result with a layer of milk

In the second attempt, a thin layer of room-temperature milk (thickness around 0.2 mm) plays the role of the scattering medium. The histogram of enhancements with 2000 samples distributed into 100 bins is given in figure 18.

A sequence of speckle patterns of light scattered by the milk sample are collected when the optimization is off. And an autocorrelation is performed in compliance with the following definition:

$$\text{Autocorrelation}(\tau) = \left\langle \frac{\sum_{i,j} (A_{i,j}(t) - \langle A(t) \rangle) (A_{i,j}(t + \tau) - \langle A(t + \tau) \rangle)}{\sqrt{\sum_{i,j} (A_{i,j}(t) - \langle A(t) \rangle)^2 \cdot \sum_{i,j} (A_{i,j}(t + \tau) - \langle A(t + \tau) \rangle)^2}} \right\rangle$$

where indexes i and j indicate the elements of an image array, τ is the shift of time, $\overline{A(t)}$ is the elementwise average of an image at time t . The highest overline indicates an average over the time sequence. The result of the autocorrelation is shown in figure 19. One can see that the typical decorrelation time scale is around 0.25s. This result agrees with the approximate conclusion in subsection 7.1. In principle, solely in terms of speed, for a dynamical sample with a decorrelation time longer than 0.25s, the setup developed in this project is capable to focus light. However, practically, speed is not the only criterion judging the applicability of this setup. A static sample with strong back-scattering or absorption is typically difficult to focus through.

Through a calculation with the theory of diffusion, one can obtain a decorrelation time with the same degree of magnitude. Light in milk is mainly scattered by lipid spheres, so one can start from looking at the Brownian motion of lipid spheres. In the Stokes-Einstein theorem, the mean square displacement is given by:

$$\langle r^2(t) \rangle = 6Dt = \frac{6k_B T}{6\pi\eta R} t$$

where $r(t)$ is the displacement varying with time, D is the diffusivity, $k_B T$ is the product of the Boltzmann constant and the temperature, $\eta \approx 3 \times 10^{-3} Pa \cdot s$ is the viscosity of milk and $10^{-5} m \leq R \leq 5 \times 10^{-5} m$ is the size of the lipid spheres in milk. Multiplying both sides with the square of the wave number $\frac{2\pi}{\lambda}$, one gets the square of the "mean square phase change" for light scattered once:

$$\left\langle \left(\frac{2\pi}{\lambda} \right)^2 r^2(t) \right\rangle = 6Dk^2 t = \frac{k_B T}{\pi\eta R} \left(\frac{2\pi}{\lambda} \right)^2 t$$

Since light is typically scattered multiple times in milk, the total "mean square phase change" needs a correction like:

$$\langle \phi_{total}^2 \rangle = \left\langle \left(\frac{2\pi}{\lambda} \right)^2 r^2(t) \right\rangle \frac{L^2}{l^{*2}} = \frac{k_B T}{\pi\eta R} \left(\frac{2\pi}{\lambda} \right)^2 t \frac{L^2}{l^{*2}}$$

where $5 \times 10^{-5} m \leq l^* \leq 10^{-4} m$ is the mean free path of light in milk, $L = 0.2 mm$ is the thickness of the milk layer. By defining the decorrelation as $\langle \phi_{total}^2 \rangle = 1$, one can estimate the decorrelation time as follows:

$$12.5ms \leq \tau = \frac{\eta R l^{*2} \lambda^2}{4\pi k_B T L^2} \leq 0.25s$$

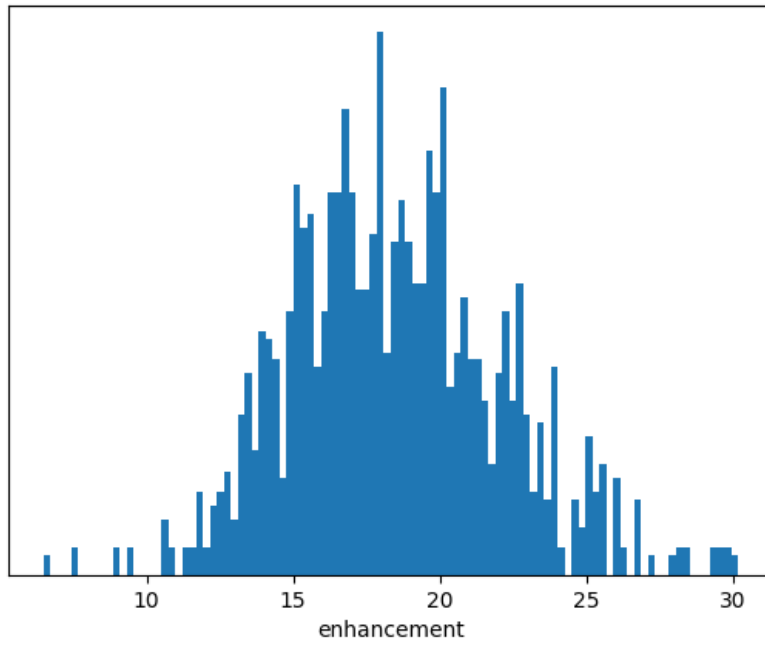
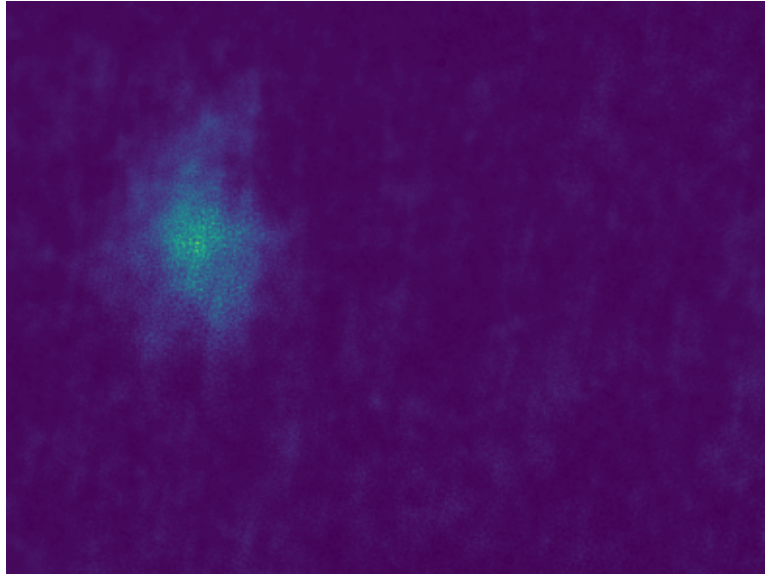
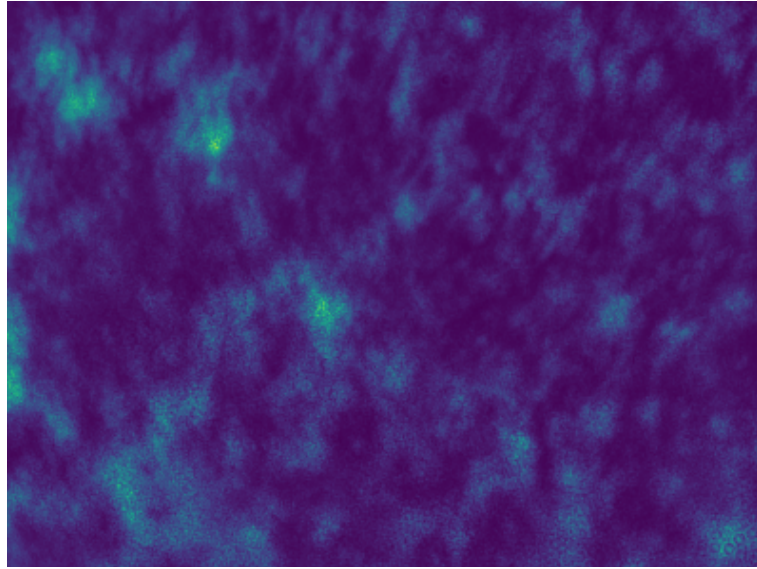
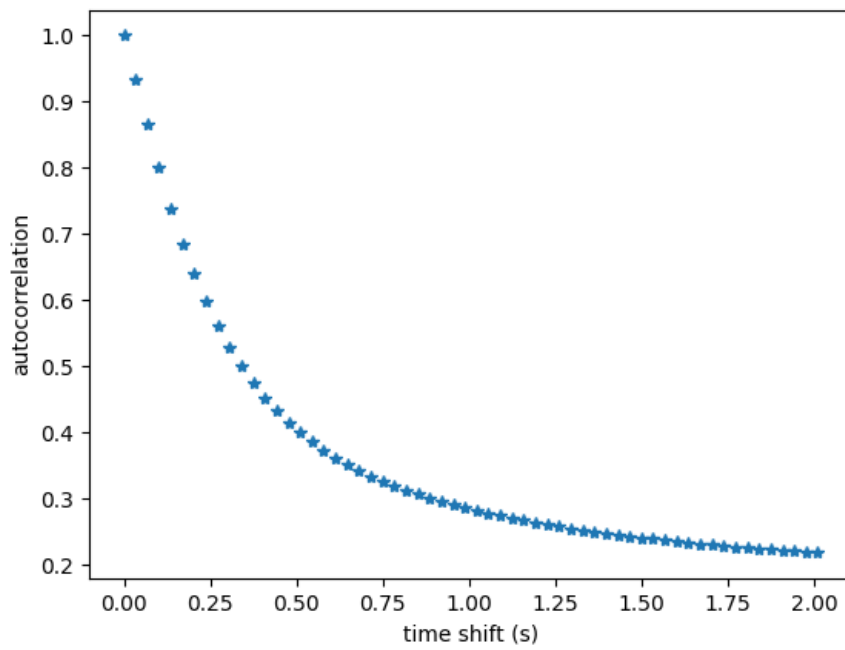


Figure 18: Result with alayer of milk



(a)



(b)

Figure 19: (a) A typical speckle pattern received behind a milk scattering sample with a thickness of 0.2mm. (b) Autocorrelation of the speckle patterns. One can find a characteristic decorrelation time around 0.25s.

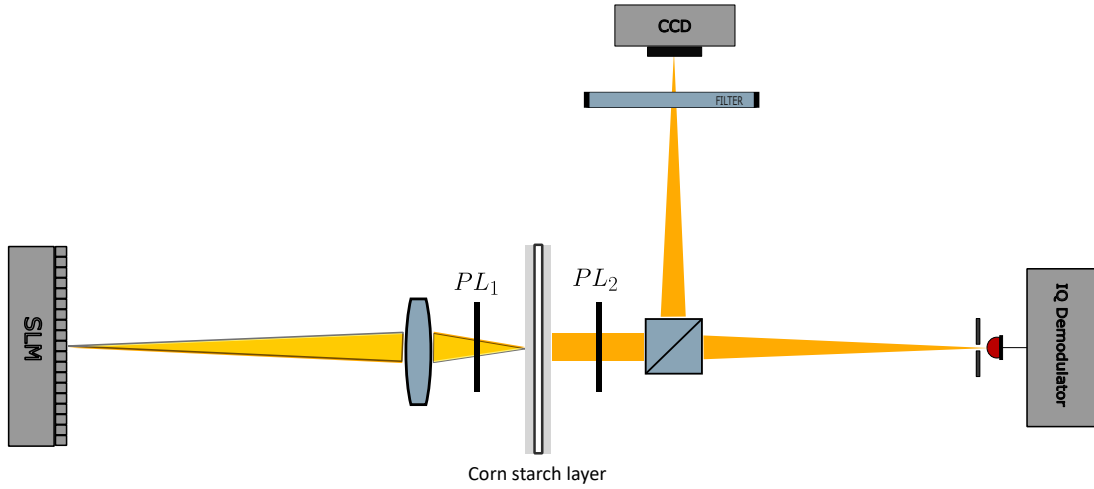


Figure 20: Focusing through a layer of corn starch

7.3 Result with a layer of corn starch

It is rather typical that the polarization of the light is modified in a multiple-scattering process. Therefore, it would be interesting to see whether one can generate a focus solely formed by the light with a linear polarization perpendicular to that of the incoming light. The setup layout for this purpose is given in figure 20. The linear polarization directions of PL1 and PL2 are perpendicular to each other.

Such a goal can be challenging for the method developed in this project due to the typically low intensity of the outgoing light with an orthogonal polarization. To overcome this, one has to prepare for a scattering sample providing with low absorption and sufficient multi-scattering. A corn starch layer with the thickness of 0.1mm fulfills the above requirements, and the result with such a sample is given in figure 21.

During the measurement, it was noticed that the beam splitter sending light to the CCD camera has the light strongly polarized. The majority of light linearly polarized in the direction of PL2 is sent to the camera while only a small portion can reach the SiPM to be used for IQ demodulation. As a result, the enhancement acquired above can be underestimated. A less polarizing beam splitter is used in the experiment introduced in section 7.4.

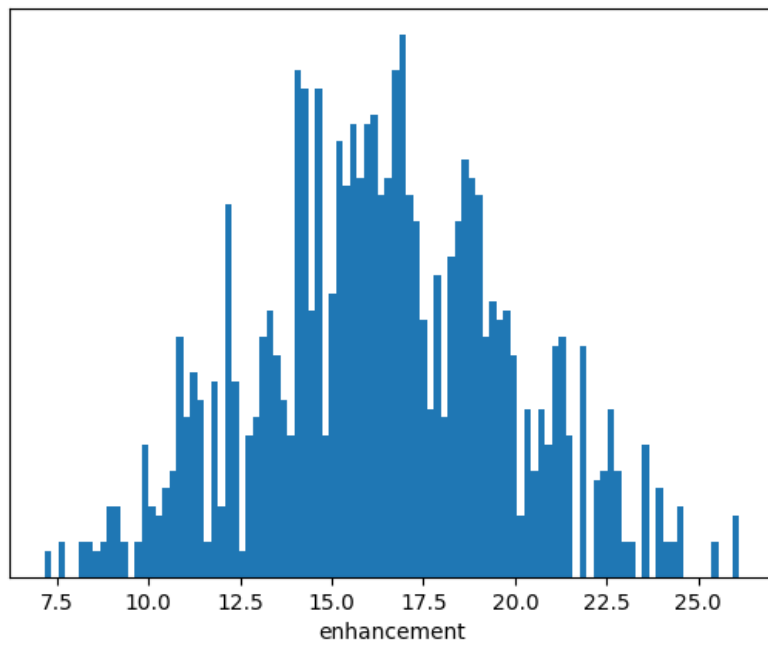
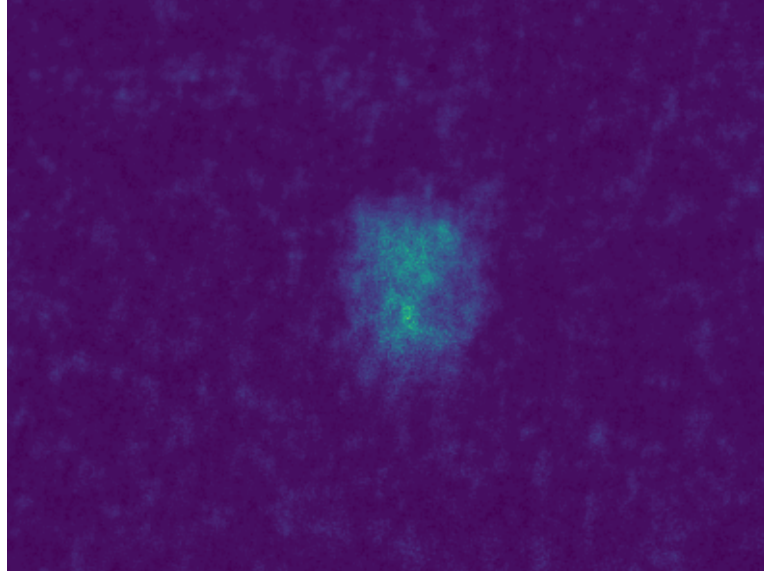


Figure 21: Result with a layer of corn starch

7.4 Result with multi-mode fibers

Compared to a thin layer of corn starch, a piece of optical fiber can have the light traveling through it more uniformly depolarized. Meanwhile, unfavorable effects such as back-scattering and absorption are typically weaker. Therefore, an attempt of performing wavefront shaping with multi-mode fibers as the scattering sample makes sense.

Since two orthogonal linear polarization components do not interfere, and the corresponding two independent sets of speckles typically do not overlap, the setup developed in this project can only optimize one of them. The setup layout is given in figure 22. Polarizers PL1 and PL2 are introduced to control the polarization to be optimized and the polarization to be observed respectively.

The optimization is first performed with a plastic-core tosilink cable with the length of 0.5m. The result is given in figure 23. Figure 23 (a) is captured when polarizers PL1 and PL2 are placed in parallel. Figure 23 (b) is captured when polarizers PL1 and PL2 are placed perpendicularly. One can notice that for multiple-scattering, the optimization for one linear polarization component generally is unable to have the perpendicular component simultaneously optimized.

The histograms in figure 23 (c) and figure 23 (d) are recorded when polarizers PL1 and PL2 are both placed vertically, while the histograms in figure 23 (e) and figure 23 (f) are recorded when polarizers PL1 and PL2 are both placed horizontally. One may notice a trend that the central positions of the distributions in (c) and (d) seem to be lower than that of (e) and (f). One can explain this by saying that the polarizing behavior of the beam splitter BS2 still exists: For horizontally polarized light, the transmission is stronger than the reflection. Therefore, more light is sent to the SiPM, and the optimization performs better. For vertically polarized light, less light is sent to the SiPM. As the consequence, the quality of the enhancement suffers.

The same optimization is also done with another cable with a length of 3m. The result is given in figure 24. Notice that the above mentioned trend still exists.

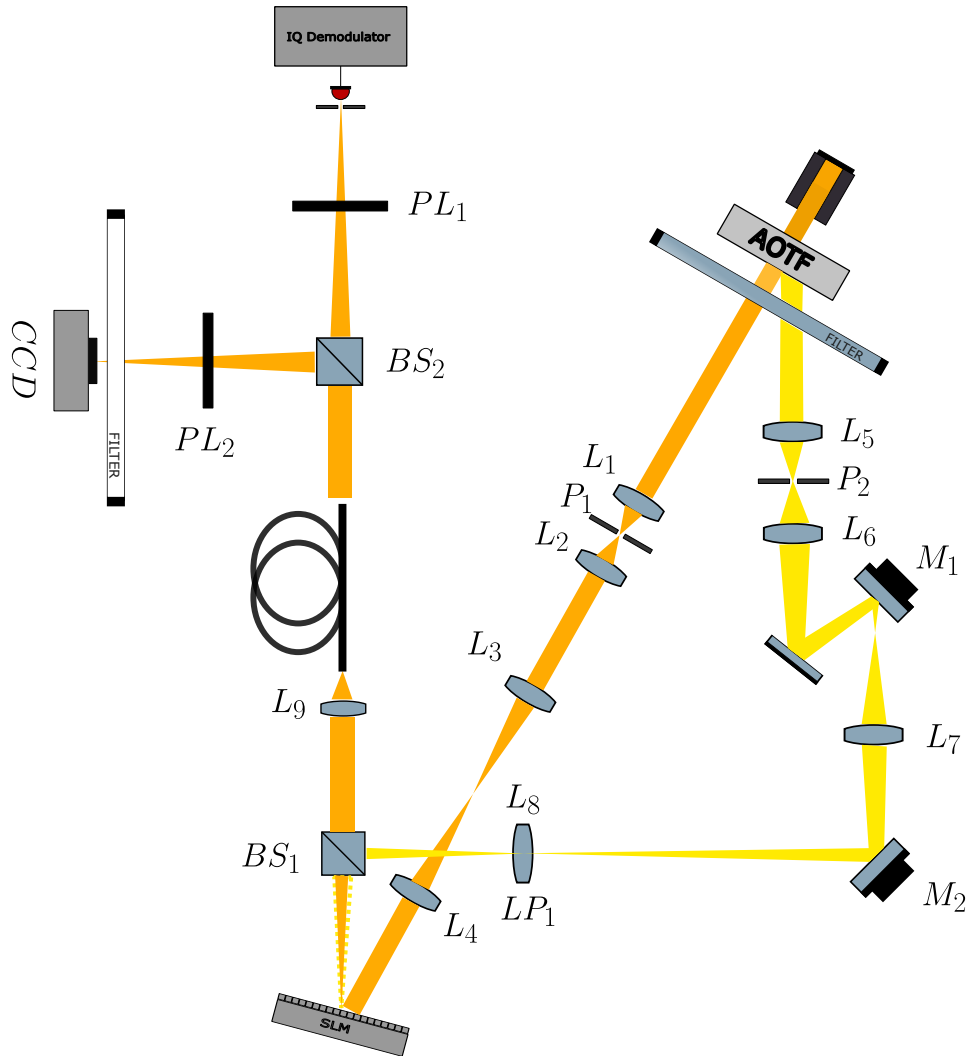
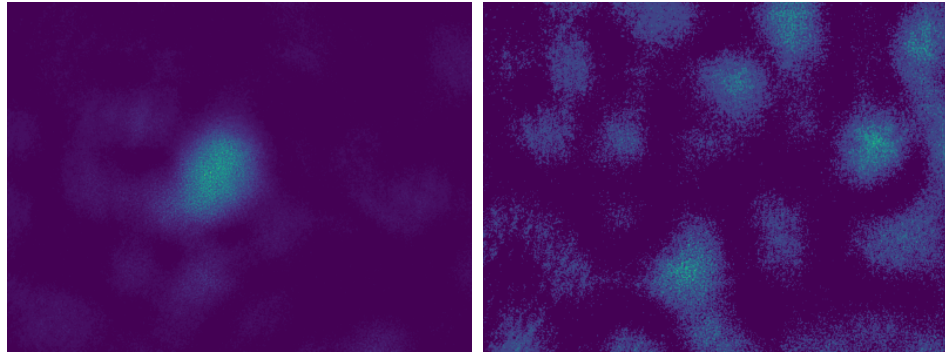


Figure 22: Focusing through multi-mode fiber



(a)

(b)

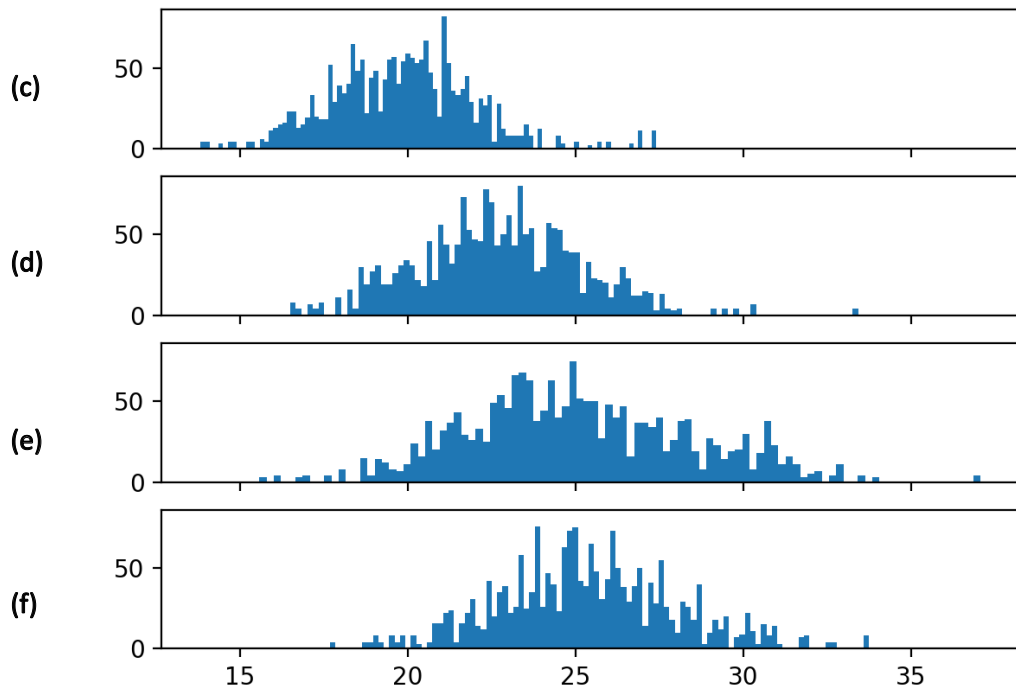


Figure 23: Result with 50cm fiber. (a) Focus generated for one linear polarization component; (b) Speckles of one linear polarization component recorded when the orthogonal component is optimized; (c) (d) Histograms of the enhancements obtained with one linear polarization component; (e) (f) Histograms of the enhancements obtained with one linear polarization component; Histograms are taken in the order (c) (e) (d) (f);

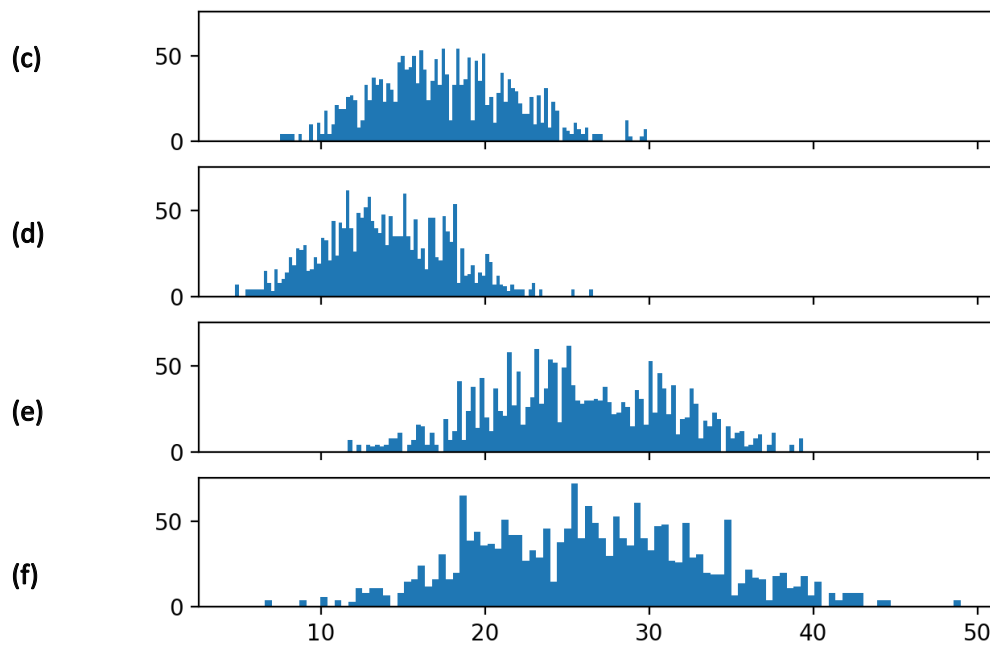
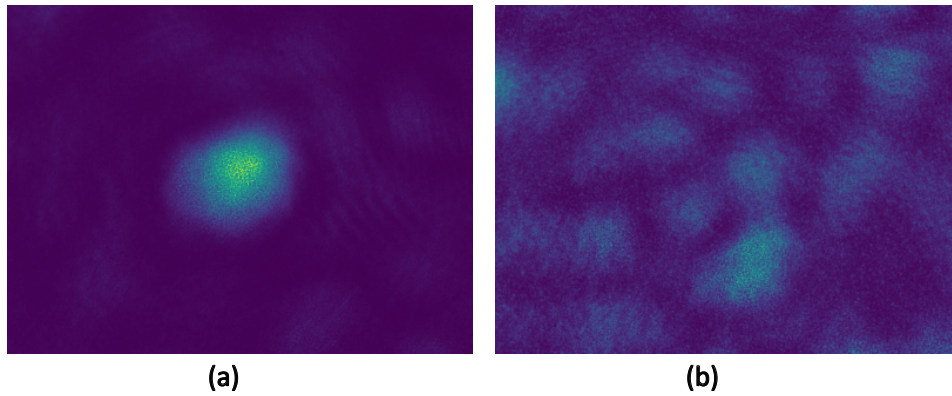


Figure 24: Result with 3m fiber. (a) Focus generated for one linear polarization component; (b) Speckles of one linear polarization component recorded when the orthogonal component is optimized; (c) (d) Histograms of the enhancements obtained with one linear polarization component; (e) (f) Histograms of the enhancements obtained with one linear polarization component; Histograms are taken in the order (c) (e) (d) (f);

8 Conclusion and outlooks

Based on interferometry and IQ demodulation, a non-iterative method for wavefront shaping is developed. The method is capable of focusing coherent light through turbid media with a speed significantly higher than that of typical traditional iterative methods. This allows light focus generation through some dynamic materials. The method also makes it more convenient (mostly faster) to study light propagation in static materials. Despite to the above achievements, the method still needs to be improved in multiple aspects:

8.1 The stability of the system

For a method having feedback loops involved, it is not surprising to see some stability problems. While the most crucial cause of the instability has not been confirmed so far, several points are considered suspicious, including the error propagation with the reference for IQ demodulation, the instability of the light source and the environmental disturbance during calibrations.

Empirically, it is found to be easier to stabilize the system by reducing the rate of update of the SLM. But this will obviously limit its application with dynamic media. Besides, turning on the laser in advance and having it stabilize itself is also beneficial for increasing the system stability.

It is possible to stabilize the reference signal by leaving some of the segments of the SLM non-updated (or only slowly updated) [8].

8.2 The observation of enhancement

As discussed in section 7.4, the polarizing feature of the beam splitter sending light to the CCD camera does not only influence the SNR of the recorded images, but also affect the optimization performance. Therefore, it would be helpful to replace the beam splitter by one not polarizing light with the currently used frequency.

The saturation of the CCD camera is found to be another problem. When the intensity of the light exceeds the upper limit of the CCD camera, the corresponding counts are allocated to the scales close to the upper limit. As a consequence, a cutoff arises in the histogram. An example is given in figure 25. Replacing the currently used optical filter in front of the CCD camera by a continuously adjustable filter wheel can help one obtain non-saturated images with relatively high SNR.

Due to the existence of dark signal and noise, the enhancement is practically calculated as:

$$Enhancement = \frac{\text{Peak intensity of smoothed focus} - \text{Averaged dark signal}}{\text{Averaged background after optimization} - \text{Averaged dark signal}}$$

where the averaged dark signal is measured in advance when the CCD camera is completely blocked. Since an averaged background after optimization is typically weak, a small change in the dark signal can lead to a rather significant change in the calculated enhancement. Unfortunately, some fluctuations in the dark signal have been noticed during the experiment. It is advisable to have it more frequently monitored and updated.

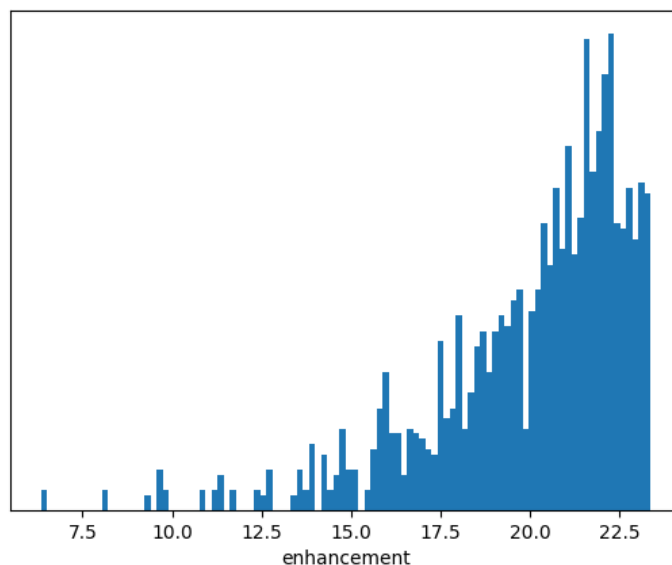


Figure 25: A histogram corresponding to a set of saturated images. A cutoff of the histogram is visible.

8.3 The speed of optimization

The speed of optimization in this project mainly has three limitations: the speed of phase acquisition at the IQ demodulator, the overwriting speed of the SLM and the speed of data transfer.

Regarding the first point, an analog IQ demodulator has been introduced to increase the speed without having the quality suffer too much [11]. Regarding the second and the third point, it had been planned to have the phase data transfer and SLM update done by scan lines instead of by arrays in order to reduce the waiting time. However, due to the stability issue mentioned above, while phase data is now transferred in scan lines, the SLM update is still done by arrays.

8.4 Focus generation in turbid media

In fields such as fluorescent microscopy, people are interested in generating light foci in turbid media instead of behind them. For traditional iterative methods, a fluorescent bead embedded in the medium can provide with sufficient feedback information. However, to perform IQ demodulation, the method developed in the project requires an object responding in a frequency of 103.086 MHz, which is typically beyond the capability of fluorescent beads.

References

- [1] Mirco Ackermann. “Experimental Investigation of Light Transport in Turbid Media”. PhD thesis. Zürich: University of Zurich, 2018. URL: <https://doi.org/10.5167/uzh-169481>.
- [2] *Adaptive Optics in Astronomy*. Cambridge University Press, 1999.
- [3] H. W. Babcock. “THE POSSIBILITY OF COMPENSATING ASTRONOMICAL SEEING”. In: *Publications of the Astronomical Society of the Pacific* 65.386 (Oct. 1953), p. 229. DOI: 10.1086/126606. URL: <https://dx.doi.org/10.1086/126606>.
- [4] Richard Davies and Markus Kasper. “Adaptive Optics for Astronomy”. In: *Annual Review of Astronomy and Astrophysics* 50. Volume 50, 2012 (2012), pp. 305–351. ISSN: 1545-4282. DOI: <https://doi.org/10.1146/annurev-astro-081811-125447>. URL: <https://www.annualreviews.org/content/journals/10.1146/annurev-astro-081811-125447>.
- [5] E. Hecht. *Optics*. Pearson Education, Incorporated, 2017. ISBN: 9780133977226. URL: <https://books.google.ch/books?id=ZarLoQEACAAJ>.
- [6] Jullien, Aurélie. “Spatial light modulators”. In: *Photoniques* 101 (2020), pp. 59–64. DOI: 10.1051/photon/202010159. URL: <https://doi.org/10.1051/photon/202010159>.
- [7] Yan Liu et al. “Focusing light inside dynamic scattering media with millisecond digital optical phase conjugation”. In: *Optica* 4.2 (Feb. 2017), pp. 280–288. DOI: 10.1364/OPTICA.4.000280. URL: <https://opg.optica.org/optica/abstract.cfm?URI=optica-4-2-280>.
- [8] Bahareh Mastiani and Ivo M. Vellekoop. “Noise-tolerant wavefront shaping in a Hadamard basis”. In: *Opt. Express* 29.11 (May 2021), pp. 17534–17541. DOI: 10.1364/OE.424147. URL: <https://opg.optica.org/oe/abstract.cfm?URI=oe-29-11-17534>.
- [9] Eyal Niv et al. “High-speed phase modulation using the DLP: application in imaging through complex media”. In: *Emerging Digital Micromirror Device Based Systems and Applications VII*. Ed. by Michael R. Douglass, Philip S. King, and Benjamin L. Lee. Vol. 9376. International Society for Optics and Photonics. SPIE, 2015, p. 937609. DOI: 10.1117/12.2080703. URL: <https://doi.org/10.1117/12.2080703>.
- [10] Jongchan Park et al. “Focusing through turbid media by polarization modulation”. In: *Opt. Lett.* 40.8 (Apr. 2015), pp. 1667–1670. DOI: 10.1364/OL.40.001667. URL: <https://opg.optica.org/ol/abstract.cfm?URI=ol-40-8-1667>.
- [11] Nehir Schmid. “Analogue signal demodulation for fast focusing through turbid media based on heterodyne detection”.
- [12] Schneider, Jale and Aegerter, Christof M. “Guide star based deconvolution for imaging behind turbid media”. In: *J. Eur. Opt. Soc.-Rapid Publ.* 14.1 (2018), p. 21. DOI: 10.1186/s41476-018-0089-5. URL: <https://doi.org/10.1186/s41476-018-0089-5>.
- [13] I. M. Vellekoop and A. P. Mosk. “Focusing coherent light through opaque strongly scattering media”. In: *Opt. Lett.* 32.16 (Aug. 2007), pp. 2309–2311. DOI: 10.1364/OL.32.002309. URL: <https://opg.optica.org/ol/abstract.cfm?URI=ol-32-16-2309>.
- [14] I. M. Vellekoop and A. P. Mosk. “Universal Optimal Transmission of Light Through Disordered Materials”. In: *Phys. Rev. Lett.* 101 (12 Sept. 2008), p. 120601. DOI: 10.1103/PhysRevLett.101.120601. URL: <https://link.aps.org/doi/10.1103/PhysRevLett.101.120601>.
- [15] Daifa Wang et al. “Focusing through dynamic tissue with millisecond digital optical phase conjugation”. In: *Optica* 2.8 (Aug. 2015), pp. 728–735. DOI: 10.1364/OPTICA.2.000728. URL: <https://opg.optica.org/optica/abstract.cfm?URI=optica-2-8-728>.

Acknowledgements

While academic writing generally requires an objective type of language, in the section of acknowledgements, it is inevitable to have one's subjective experience involved, which requires more subjective expressions. Therefore, in but only in this section, the person who drafts this thesis paper would need to use first-person (possessive) pronouns.

- I would like to acknowledge and express my sincere thanks to Prof. Dr. Christof Aegerter, the supervisor of this thesis project, who offered me the opportunity of doing this project and the necessary supports to carry it out. I have benefited significantly from his advice and elegant explanations for topics in different areas of Physics. He has set a very model for me of being a critical thinker.

Besides, I am also grateful for his coffee machine, his leather couch and his habit of not locking his office, making the above two objects always accessible.

- I would like to thank Dr. Mirco Ackermann for his instructions, technical supports and patience in explaining complicated concepts. I do appreciate the hours he spent on helping me with coding and the construction of the setup.

Beyond the academic activities, Dr. Ackermann also indirectly stimulated my motivation for coming to the campus by bringing snacks and beer to the office.

- Finally, I would also like to express my thanks to my parents, my cats, cat Garfield in the Bächlerstrasse neighbourhood and my friends at Akademischen Fechtclub Zürich (AFZ) and Armbrustschützenverein Opfikon (ASVO) for their substantial and spiritual support.